frontiers | Frontiers in Earth Science

TYPE Original Research
PUBLISHED 12 January 2023
DOI 10.3389/feart.2022.1107495

Check for updates

OPEN ACCESS

EDITED BY
Dario Gioia,
Institute of Cultural Heritage Sciences (CNR), Italy

REVIEWED BY
Giuseppe Corrado,
University of Basilicata, Italy
Domenico Chiarella,
University of London, United Kingdom

*CORRESPONDENCE
Lei He,
hel_qimg@sina.com

SPECIALTY SECTION
This article was submitted to Quaternary Science, Geomorphology and Paleoenvironment, a section of the journal Frontiers in Earth Science

RECEIVED 25 November 2022
ACCEPTED 29 December 2022
PUBLISHED 12 January 2023

CITATION
He L, Ye S, Xue C, Zhao G, Yang S and Amorosi A (2023), Sedimentology and evolution of the Holocene radial tidal sand ridge in the south Yellow Sea, China. *Front. Earth Sci.* 10:1107495. doi: 10.3389/feart.2022.1107495

COPYRIGHT
© 2023 He, Ye, Xue, Zhao, Yang and Amorosi. This is an open-access article distributed under the terms of the Creative Commons Attribution License (CC BY). The use, distribution or reproduction in other forums is permitted, provided the original author(s) and the copyright owner(s) are credited and that the original publication in this journal is cited, in accordance with accepted academic practice. No use, distribution or reproduction is permitted which does not comply with these terms.

Sedimentology and evolution of the Holocene radial tidal sand ridge in the south Yellow Sea, China

Lei He[1,2]*, Siyuan Ye[1,2,3], Chunting Xue[1], Guangming Zhao[1,2], Shixiong Yang[1,2] and Alessandro Amorosi[4]

[1]Key Laboratory of Coastal Wetland Biogeosciences, Qingdao Institute of Marine Geology, China Geological Survey, Qingdao, China, [2]Laboratory for Marine Geology, Laoshan Laboratory, Qingdao, China, [3]Institute of Marine Science and Technology, Shandong University, Qingdao, China, [4]Department of Biological, Geological and Environmental Sciences, University of Bologna, Bologna, Italy

The radial tidal sand ridge (RTSR) off the Jiangsu Coast in the south Yellow Sea is one of the most fantastic and unique natural landscapes in the world. A large number of investigations on geomorphology and marine geology have been implemented during the last several decades. The formation and evolution of the RTSR, however, are still under debate. To resolve this issue, 10 ~30–60 m-long cores were retrieved from the Jiangsu coastal plain and offshore sand ridge field in 2018–2019. Stratigraphic transects chronologically constrained by abundant radiocarbon dates were built based on sedimentological and paleoecological (i.e., foraminifer) data from selected cores. Combined with well-documented core stratigraphy from earlier studies, an age–depth plot with a local sea-level change curve revealed that the RTSR initiated approximately 9,000 cal a BP in a sandy bedform shape under transgressive conditions, continued throughout the Holocene, but developed mostly after 1128 AD, when the Yellow River flowed southward into the Yellow Sea. Abundant sediment supply, thus, appears to have played a major role in the formation and evolution of the RTSR in the south Yellow Sea.

KEYWORDS

tidal sand ridge, sedimentary evolution, south Yellow Sea, Yellow River, age–depth curve

1 Introduction

Shelf sand ridges having longitudinal crests that are over tens of kilometers long with spacings of hundreds to thousands of meters are well known from ancient and modern continental margins (Emery, 1968; Johnson, 1977; Brenner, 1980; Wagle and Veerayya, 1996; Park et al., 2003; Wu et al., 2017; Chiarella et al., 2020; Longhitano et al., 2021). They generally form parallel to the dominant current flow on sediment-laden shelves, regardless of tidal or storm origin (Houbolt, 1968; Swift, 1975; Swift et al., 1978; Stride, 1982). Well-documented examples of tide-dominated shelf sand ridges have been reported from the south-eastern North Sea (Davis and Balson, 1992; Trentesaux et al., 1999), the English Channel and the Celtic Sea between Ireland and France (Berne et al., 1998; Reynaud et al., 1999), the western Yellow Sea off China (Liu et al., 1989; Li et al., 2001), the inner shelf off Korea (Park and Lee, 1994; Chough et al., 2004), the southern Yellow Sea and the East China Sea (Yang, 1989; Berne et al., 2002; Liu et al., 2007), the Bohai Strait (Liu et al., 1998), the Taiwan Strait (Liao and Yu, 2005), and the southwest Florida inner shelf (Davis et al., 1993). Storm-dominated sand ridges have been described in the U.S. Atlantic Bight (Swift and Field, 1981; Goff et al., 1999; Snedden et al., 2011), the Brazilian shelf (Figueiredo et al., 1982), the Argentinean shelf (Parker et al., 1982), the Japanese Sendai shelf (Saito, 1989), the Canadian shelf (Hoogendoorn and Dalrymple, 1986),

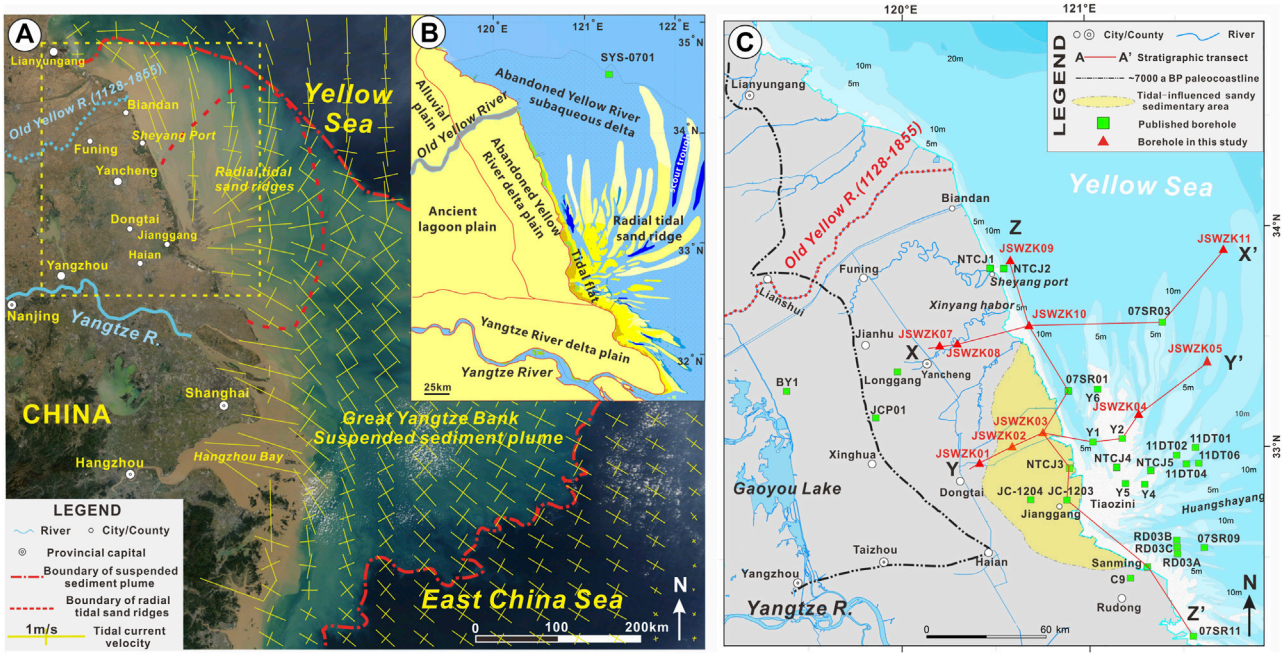

FIGURE 1
Radial tidal sand ridge and distribution of borehole data in this study. **(A)** Remote sensing satellite map of the Yellow Sea and East China Sea captured by NASA's Terra satellite at 9 November 2017. Notice that the suspended sediment plume of the great Yangtze bank and radial tidal sand ridges is outlined by the red dashed–dotted line and the dotted line, respectively. The yellow cross lines represent the distribution of M2 current ellipses (crosses) and magnitudes of semi-major axes (Uehara et al., 2002). **(B)** Schematic map of geological sedimentary units in the study area, modified from Li et al. (2001) and Xue et al. (2010). **(C)** Distribution of 10 boreholes and other previously published boreholes in the north Jiangsu coastal plain and in the radial tidal sand ridge region. The black dashed–dotted line represents the limit of the Holocene maximum transgression in the northern Jiangsu Coast (Xue et al., 2010). The red dashed line indicates the old Yellow River course between 1128 and 1855 AD.

the central Dutch coast (van de Meene and van Rijn, 2000), the German shelf (Antia, 1996), and the West Florida shelf (Twichell et al., 2003; Knobles et al., 2008).

Surface characteristics of shelf sand ridges have been extensively studied since the early 1970s by using various techniques in the hot-spot region, such as the U.S. Atlantic Bight (Swift et al., 1972; Goff et al., 1999; Pendleton et al., 2017). Early approaches to shelf sand ridges mainly focused on acoustic observations and surficial sampling (Green, 1986; Davis and Balson, 1992). Further progress in understanding the origin and evolution of shelf sand ridges was derived from the measurement of high-resolution seismic profiles and longer vibracores with a few radiocarbon dates (Park et al., 2006; Snedden et al., 2011). Recent studies of sand ridges have gradually turned to hydrodynamic model simulations, *in situ* underwater video camera observations, and remote sensing satellite monitoring (Vis-Star et al., 2007; Shi et al., 2011; Yoshikawa and Nemoto, 2014).

Previous studies have documented that shelf sand ridges predominantly occur in passive continental margins and broad continental shelf areas (Amos and King 1984; Snedden and Dalrymple 1999). Their morphological characteristics are closely related to the dominant ocean current (Galloway and Hobday, 1983) and are controlled by geologic (i.e., relative sea-level rise, shoreline transgression, and antecedent morphological relief), oceanographic (i.e., storms, tidal currents, and offshore-directed currents), and other (i.e., sediment supply and net sediment transport direction) processes (McBride and Moslow, 1991; Park et al., 2006; Nnafie et al., 2014; Ridente, 2018). However, two different hypotheses have been proposed for the origin of shelf sand ridges. The first hypothesis states that they represent relict features of the transgression, such as deltas or estuarine shoals, which became stranded, eroded, reworked, and then eventually submerged after a relative sea-level rise (McClennan and McMaster, 1971; McBride and Moslow, 1991). An alternative thought is that sand ridges were formed and stabilized by post-transgressive oceanographic processes related to the inherent dynamic interactions between the hydrodynamic force and sandy beds (Swift and Freeland, 1978; Trowbridge, 1995; Twichell et al., 2003). High-resolution seismic measurements in various sea regions supported the relict hypothesis (Berne et al., 1998; Jung et al., 1998; Park et al., 2006), whereas numerical modeling and hydrodynamic simulations were in favor of the hydrodynamic hypothesis (Calvete et al., 2001; Uehara et al., 2002; Vis-Star et al., 2007). A lack of studies on Holocene stratigraphic sequences with accurate chronological constraints in shelf sand ridge regions might explain these different views (Ridente, 2018).

The radial tidal sand ridge (RTSR) off the Jiangsu Coast in the south Yellow Sea is one of the world's unique geomorphic units. It is famous for its radial current pattern, which includes dozens of large either subaerial or subaqueous radial sand ridges and high suspended sediment concentrations (Figure 1A; Wang, 2002; Liu and Xia, 2004). To understand the origin and mechanism of this unique unit, a variety of field investigations have been carried out in this region since the 1960s, including geomorphology, geology, meteorology, hydrology, and sediment dynamics (see the summary in Wang Y. et al., 2012).

Since then, a large number of papers have been published on sand ridge morphology, sediment characteristics and provenance, sedimentary dynamic mechanisms, sand ridge migration, and genetic models (Geng et al., 1983; Wang et al., 1999; Li et al., 2001; Yin et al., 2008; Yin et al., 2016; Gao, 2009; Wang Y. et al., 2012; Zhang C. et al., 2013; Rao et al., 2015; Xu et al., 2019; Liu et al., 2021). However, the timing and mechanisms of formation of the Jiangsu radial tidal sand ridge are still largely under debate (Li and Zhao, 1995; Wang et al., 1998; Li and Yin, 2013; Yin et al., 2016). Several cores with long-time sequences, accurate dating, and seismic profiles have been documented in detail in this region (Sun et al., 2015; Yin et al., 2016). Nevertheless, these data clarified neither the origin nor the timing of formation of the RTSR, due to lack of detailed sea–land stratigraphic correlation, especially from the tidal sandy coast to the inner-shelf sand ridge (see the "tidal-genetic sandy deposition" in Li et al., 2001). Based on the analysis of sedimentary facies, stratigraphy and relatively precise chronology from 10 ~30–60 m-long cores recovered in the Jiangsu coast plain and in the radial sand ridge region in 2018–2019 (Figure 1C), and numerous previously published boreholes, this study aims to 1) reconstruct the detailed stratigraphic architecture from the coastal plain to the sand ridge region, 2) examine its late Pleistocene evolution, and 3) explore the mechanisms and timing of formation of the Jiangsu radial tidal sand ridge.

2 Geological setting

2.1 Modern radial tidal sand ridge off the Jiangsu Coast

The modern RTSR distributes at the apex of Jianggang (town) and forms a radial underwater topography with alternating ridges and troughs off the Jiangsu Coast in the south Yellow Sea (Figure 1B). Sand ridges are ~260 km long in the N–S direction and over 150 km long in the W–E direction, with a total area of ~30,000 km^2 (Liu and Xia, 2004). More than 70 sand ridges alternating with tidal current channels have been identified in this area. At least 19 large-scale submarine sand ridges were found, most of which are ~10–100 km in length and ~10–15 km in width. The depth of tidal current channels between sand ridges is ~10–30 m, and the maximum depth is ~48 m (Wang, 2002).

Sand ridges at the apex (Jianggang) are cut by grooves, and sand bodies are small, diverse, and disordered (i.e., a length of ~4.4 km around Tiaozini, Figure 1C), whereas sand ridges are well developed with an average of ~52 km in 13 major ridges outside the apex (Wang, 2002). The heads and tails of each sand ridge are narrow (mostly <2 km), whereas the middle parts are wide (~15 km wide in the major ridges (Liu and Xia, 2004)). Within each sand ridge, the head has the highest elevation. As the sand ridge extends outward, its elevation also decreases. The troughs between sand ridges become wider and deeper from the shallow to the deep sea (Ren, 1986).

Bounded by Jianggang, the north slope of the sand ridges is steeper than the south slope on the northern side of Jianggang (Figure 1C). Sand bodies are large and densely distributed, and troughs are generally shallow. As troughs in the NE direction are adjacent to the open sea, erosion is present on both sides of the sand ridges and troughs, and sand ridges gradually retreat and disappear (Wang et al., 2004). On the southern side of Jianggang, in general, the southern slopes of the sand ridges are steeper than the northern slopes. This region is characterized by low sediment accumulation and erosion with scattered deep troughs. The coastal tidal flat gradually silts into the sea, and a new sand ridge is formed at the top of the tidal channel. Even so, the overall deposition pattern is relatively stable in the southern region (Wang, 2002).

Sediment at the surface of the sand ridges generally consists of well-sorted fine sand and silty sand within 100 km of the apex (Wang, 2002). The proportion of fine sand is >80%, including the sand ridges and tidal current channels (Liu and Xia, 2004). Low-lying sectors contain small amounts of silt, whereas in tidal current channels, gravelly sand is quite abundant (~29%) with medium grain sizes between 1.2 Φ and 2.6 Φ in local major channels, and grain size becomes smaller (2.9–5.0 Φ of medium grain sizes) at both sides (Wang et al., 1999; Wang, 2002). Clayey silt is distributed in the outermost parts of the sand ridge region, where water depth is commonly 18–20 m. The radial apex is generally composed of silty sand and sandy silt and turns to a muddy tidal flat landward. On the whole, grain size gradually decreases from the core area to the periphery of the RTSR, which is consistent with the pattern of hydrodynamic strength (Liu and Xia, 2004).

2.2 Coastal hydrology of the south Yellow Sea

The study area is adjacent to the south Yellow Sea (SYS), where tidal currents, waves, and coastal currents are prevailing (Figure 1A). The Yellow Sea is a semi-enclosed sea that is generally influenced by two types of tidal waves: a progressive tidal wave from the Western Pacific region and a local reflected tidal wave formed by the obstruction of the Shandong Peninsula in the northwest (Zhang et al., 1999; Su and Yuan, 2005). These two tidal waves converge offshore the Jiangsu Coast in the south Yellow Sea, forming the rotating tidal wave systems and the radial tidal field in the north and east of Jianggang (Wang, 2002).

The Jiangsu coastal area generally rules the regular semidiurnal tide, with very short duration (an average of ~.38 h) between tidal rise and fall (Wang, 2002). In addition, the onshore shallow water area and radial sand ridge field, such as Xinyang Harbor and Jianggang, rule the irregular semidiurnal tide with a relatively long duration (4–5 h) (Liu and Xia, 2004). Tidal ranges normally average 2.5–4 m in the study area but can reach up to 9.28 m in the Huangshayang Channel, which is the maximum value recorded in the China Seas (Ye et al., 1988). In the RTSR field, tidal currents are very strong, averaging a velocity of ~1.5–2 m s^{-1} in the spring tidal current, with a maximum tidal current velocity exceeding 4.0 m s^{-1} (Wang, 2002).

The Jiangsu Coast is primarily affected by northward and northeastern main waves, with remarkable seasonal changes. Wind-induced waves commonly go toward the southeast during the summer, whereas waves from northerly and northeasterly directions prevail in the winter (Wang Y. et al., 2012). The height of wind-induced waves ranges between .5 m and 3 m in this region, occasionally exceeding 4 m during typhoons and severe storms (Liu and Xia, 2004; Liu et al., 2010).

The oceanic circulation in the SYS generally includes the Yellow Sea Warm Current (YSWC) and Shandong–Jiangsu coastal currents (Su and Yuan, 2005). The YSWC is a branch of the Kuroshio Current that carries warm and salty water northward into the Yellow Sea (Lan et al., 1986). In the China Seas, coastal currents with relatively low salinity due to the input of riverine water typically flow southward in

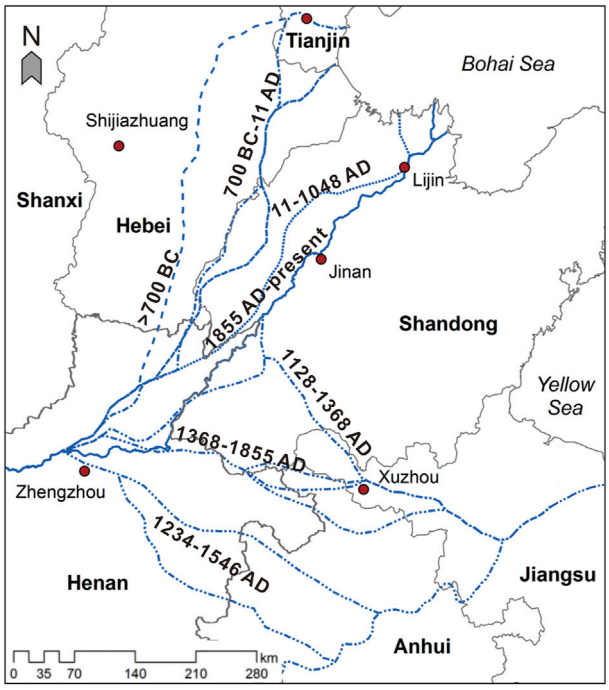

FIGURE 2
River diversion of the Lower Yellow River course in recorded history modified from Xue et al. (2003), Wang and Su (2013). Despite the Yellow River changing its course southward to Yellow Sea several times, the overall flowing time is limited between 1128 and 1855 AD.

winter and northward in summer. However, the YSWC is too weak to reach north of 35°N in summer because the southward-flowing cold water mass in the central SYS hinders the warm currents (Su and Yuan, 2005). Given the northward and northeastern main waves in the Jiangsu Coast throughout the year, the Jiangsu coastal currents flow persistently southward during both summer and winter (Beardsley, 1983). Recent studies of green tide (*Enteromorpha prolifera*) along the Jiangsu–Shandong coast revealed that coastal currents may flow northeast for a short period during the summer (Lee et al., 2011; Song et al., 2018).

2.3 River diversion of the lower Yellow River courses since 20 ka BP

The Yellow River is well known for its high sand content (Ren and Shi, 1986). The annual sediment load carried by the Yellow River has been ~1.1 × 10^9 tons over the past 2,000 years (Wang et al., 2007a). When the Yellow River flowed through the central mountain area into the flat, lower alluvial plain, it easily plugged and breached; therefore, its lower reaches migrated because of its huge sediment load (Cheng and Xue, 1997; Wang et al., 2007a). Previous studies revealed that at least seven times of major diversions occurred in the lower Yellow River course over recorded history (Xue et al., 2003; Wang and Su, 2013), with the river flowing north into the Bohai Sea and south through the Huaihe River into the south Yellow Sea (Figure 2).

It is to be noted that no direct sedimentary record suggests that the Yellow River delivered sediments into the south Yellow Sea during the Holocene, except for 1128–1855 AD. Instead, since 7,000 a BP, the Yellow River has entered the Bohai Sea and formed at least seven phases of deltas in the Bohai Coast (Xue, 1993; He et al., 2019). During the early Holocene, the Yellow River appeared to flow through the Bohai Strait into the north Yellow Sea, forming the Shandong mud–clinoform deposits during 9,600–5,000 a BP (Liu et al., 2004; Liu et al., 2010; Xue et al., 2018). Recent study of the ancient river channel in the Bohai Bay revealed that the ancient Yellow River seems to pass through the Bohai Bay and flow eastward consistently between 21.8 and ~9 ka BP (Lei et al., 2021), although some research studies on Late Pleistocene losses in the Huaihe River Basin implied that the Yellow River may partly go across the Huaihe River Basin and empty into the south Yellow Sea during the MIS 2 (marine isotope stage 2) period (~13.2 ka BP) (Zhang et al., 2016).

2.4 Abandoned Jiangsu Yellow River Delta

To hold back the invasion of the Jurchen army from North China, many dykes in the south bank of the Yellow River were artificially destroyed at 1128 AD in central Henan Province, resulting in a major southward shift of the Yellow River Channel since then (Figure 2; Liu et al., 2013). During a period of more than 700 years (1128–1855 AD), the Yellow River captured several tributaries of the Huaihe River and emptied into the Yellow Sea, where it formed a large delta lobe along the Jiangsu Coast (Xue et al., 2003; Xue et al., 2011). Furthermore, the Yellow River largely shifted its course from the Yellow Sea back to the Bohai Sea after 1855 AD, leading to the abandonment of the Jiangsu Yellow River Delta.

The terrestrial part of the abandoned Jiangsu Yellow River Delta is distributed on the east side of 1128 AD ancient shoreline in northern Jiangsu (Figure 1B). Bounded by the old Yellow River mouth, an asymmetrical, long-oval shape of deltaic bodies was formed, of which the southern part may extend to the Jianggang area under the action of the consistently southward longshore current, and the northern part expands to the Lianyungang region (Figure 1B; Xue et al., 2010; Liu et al., 2013). Additionally, the proximal subaqueous Jiangsu Yellow River Delta is mainly distributed near the abandoned Yellow River mouth, but the distal part is widely dispersed on the broad shelf of the south Yellow Sea and can even be transported to the slope of the platform edge (water depth below 20 m) under the action of late erosion (Liu et al., 2010; Zhou et al., 2014). Up until now, the boundary between the abandoned Jiangsu Yellow River Delta and the radial tidal sand ridge is not exactly defined in the study area, no matter whether it is on the shoreface or offshore (the south Yellow Sea shelf). Previous studies commonly recognized the dividing line of clayey silt/sand as the boundary, which approximately distributes eastward along the Xinyang Harbor (Li et al., 2001; Liu et al., 2010).

3 Materials and methods

A total of 10 cores, each 90 mm in diameter, were retrieved from the Jiangsu coastal plain and radial tidal sand ridges by rotary drilling in 2018–2019 (Figure 1C). Their coordinates, elevations, lengths, and coring recovery rates (always >90%) are summarized in Table 1. The lithology of each core as well as its sediment color, composition, sedimentary structures, bedding, grain size, and fossils was examined to identify the sedimentary facies.

TABLE 1 General information about the 10 cores investigated in this study.

Core	Coordinate		Elevation (m)	Length (m)	Recovery rate (%)
	Latitude (N)	Longitude (E)			
JSWZK01	32°56′31.36″	120°24′57.78″	3.15	31.8	92.8
JSWZK02	33°00′58.25″	120°35′30.02″	3.18	33.3	96.8
JSWZK03	33°04′41.73″	120°45′28.32″	3.26	61.4	98.2
JSWZK04	33°09′27.62″	121°16′25.27″	−4.2	40.9	91.6
JSWZK05	33°23′27.09″	121°38′53.21″	−20.1	40.7	90.3
JSWZK07	33°28′27.65"	120°12′02.54"	1.88	31.7	94.0
JSWZK08	33°28′58.19"	120°17′54.12"	2.11	32	96.8
JSWZK09	33°51′33.69"	120°35′12.94"	−13.7	30.1	95.0
JSWZK10	33°33′51.81"	120°41′11.10"	−9.5	30.3	94.0
JSWZK11	33°53′56.14"	121°44′40.74"	−18.6	30.2	90.5

A total of 54 samples were collected and analyzed for ^{14}C dating with an accelerator mass spectrometer (AMS) by Beta Analytic (Miami) and Pilot National Laboratory for Marine Science and Technology (Qingdao), respectively. These samples included mollusk shells, plant fragments, organic matter, and organic sediments. Age determinations were based on a Libby half-life of 5,568 years. Radiocarbon ages were corrected for the regional marine reservoir effect ($\Delta R = -100 \pm 36$ a), a regional average determined for the Yellow Sea by Southon et al. (2002), and calibrated using Calib Rev. 7.02 with one standard deviation (1σ) uncertainty (Reimer et al., 2013).

A total of 23 samples were collected for optically stimulated luminescence (OSL) dating from relatively homogeneous silty-sandy layers. Each sample was sealed into two black, opaque cartridges, 6 cm in height and 3.5 cm in diameter, in a dimly lit environment. All samples were kept in shockproof and lightproof bags and finally examined in the Inspection & Test Center of Marine Geology (Ministry of Natural Resources of China), using the method of Murray and Wintle (2000). The contents of U and Th required for dose rate calculation were obtained by a CANBERRA-E3830 high-purity germanium γ spectrometer, while the content of K was detected by an IRIS Intrepid II XSP plasma emission spectrometer. The equivalent dose was obtained using the Lexsyg research luminescence meter, and the experimental excitation light source was a blue light diode ($\lambda = 470 \pm 30$ nm), with the instrument's irradiation source being 90Sr/90Y.

About 800 samples were collected for grain size analysis in cores JSWZK01, JSWZK03, and JSWZK07. The average sampling interval was ~.15 m. The weight of each sample was about 10 g. Grain size was determined using a Mastersizer 2000 laser particle size analyzer after pre-treating with 10% H_2O_2 and .10 N HCl to remove organic matter and carbonates. The range of particle sizes was .02–1,000 μm; standard deviations were <1% of the mean values; and reproducibility (φ50) was also <1%. Grain-size classification was based on the Krumbein phi (Φ) scale (Krumbein and Sloss, 1963). Size parameters were calculated based on the methods of Folk and Ward (1957).

A total of ~300 foraminiferal samples were collected in cores JSWZK01, JSWZK03, and JSWZK07. The average sampling interval was ~.2 m in silty and muddy layers and ~1 m in sandy beds. All samples were dried at 50°C in an oven and weighed at around 50 g per sample. About 10% H_2O_2 was added to soak the sediment for full dispersion and then washed over a 63-μm sieve. After drying, foraminifera were concentrated and separated using the CCl_4 flotation method (Wang et al., 1985). Sample subdivision was carried out when the foraminiferal abundance of a sample was very high. A representative number of more than 200 individuals was commonly obtained for each assemblage. Otherwise, all available tests were picked and identified under a Zeiss optical stereoscope. The "foraminiferal abundance" parameter in this study is the number of foraminifera per 50 g of dry sediment. The "simple diversity" is the number of foraminiferal species in each sample.

4 Results

4.1 Dating results

Tables 2, 3 list 54 radiocarbon dates and 23 OSL ages that were obtained from the 10 boreholes in the Jiangsu coastal plain and radial tidal sand ridges. For radiocarbon dating results, about three-quarters of these data are less than 10,000 years old, which are mostly reliable except for a few reversals (old layers at young ages; see the similar reversals in Stanley and Chen, 2000). The remaining quarter of dating ages are more than 35,000 years old, close to the carbon-14 dating limit. These old data, which are usually collected from deep sampling points, can only be used for reference purposes.

For OSL ages, similarly, more than two-thirds of the dates are less than 100 ka old, which is within the range of confidence. The rest is more than 100 ka old, even older than 150 ka, which exceeds the OSL dating limit and can only be used for reference.

4.2 Sedimentary facies

A total of 12 facies associations (hereinafter called "facies," Figure 3) were grouped into five depositional systems (alluvial,

TABLE 2 Radiocarbon dating results of 54 samples from the investigated boreholes.

Core	Sample	Depth (m)	Lab no.	Materials	$\delta^{13}C$ (per mil)	Conventional age	Calendar ages (cal a BP)	
						(a BP)	Intercept	Range (1σ)
JSWZK01	J1S01	1.95	510290	Organic sediment	−20.1	4,620 ± 30	5,410	5,308–~5,445
	J1S02	10.88	510291	*Potamocorbula laevis*	1.0	7,630 ± 30	8,205	8,151–~8,273
	J1S03	11.7	510292	*Pelecyora trigona*	−1.7	7,440 ± 30	7,995	7,936–~8,041
	J1S05	12.54	Q200206	*Ruditapes philippinarum*	—	5,670 ± 25	6,195	6,160–~6,260
	J1S04	13.3	510293	*Potamocorbula laevis*	−.5	7,620 ± 30	8,190	8,140–~8,269
JSWZK02	J2S01	3.3	510294	Organic sediment	−23.7	3,290 ± 30	3,520	3,480–~3,560
	J2S02	12.36	510295	Plant materials	−25.9	8,570 ± 30	9,540	9,529–~9,545
	J2S05	14.82	Q200456	Organic matters	−25.5	9,156 ± 40	10,325	10,246–~10,377
	J2S03	24.76	510296	Plant materials	−28.9	7,820 ± 30	8,600	8,578–~8,628
	J2S04	31.58	510297	Plant materials	−25.9	11,080 ± 30	12,955	12,897–~13,028
JSWZK03	J3S01	7.35	510298	Shell fragments	2.8	1,480 ± 30	1,140	1,079–~1,204
	J3S02	11.88	510299	Shell fragments	0.0	1,620 ± 30	1,275	1,231–~1,318
	J3S03	24.7	510300	Plant materials	−26.7	8,880 ± 30	10,030	9,918–~10,149
	J3S04	36.93	510301	Plant materials	−27.4	>43,500		
	J3S05	57.16	510302	Oyster fragments	−3.2	>43,500		
JSWZK04	J4S01	4.85	510303	Organic sediment	−20.8	8,720 ± 30	9,665	9,597–~9,705
	J4S02	7.12	510304	Organic sediment	−21.5	10,480 ± 30	12,465	12,404–~12,527
	J4S03	12.55	510305	Organic sediment	−22.4	9,660 ± 30	11,110	10,898–~11,173
	J4S06	16.76	Q200215	*Arca subcrenata*	—	2,695 ± 20	2,515	2,475–~2,645
	J4S04	17.18	510306	Oyster fragments	.9	5,170 ± 30	5,630	5,578–~5,671
	J4S05	29.9	510307	*Corbicula fluminea*	−9.1	>43,500		
JSWZK05	J5S01	.69	510308	Shell fragments	−1.1	3,580 ± 30	3,590	3,534–~3,667
	J5S02	5.62	510309	Shell fragments	−2.5	5,420 ± 30	5,905	5,859–~5,967
	J5S03	9.15	510310	*Potamocorbula laevis*	−.6	8,440 ± 30	9,175	9,100–~9,253
	J5S04	11.7	510311	Oyster fragments	.9	8,790 ± 30	9,535	9,482–~9,582
JSWZK07	J7S01	8.88	542791	Organic matters	−29.0	50 ± 30	145	31–~256
	J7S02	14.34	542792	Plant materials	−27.9	6,390 ± 30	7,320	7,270–~7,368

(Continued on following page)

10.3389/feart.2022.1107495

TABLE 2 (*Continued*) Radiocarbon dating results of 54 samples from the investigated boreholes.

Core	Sample	Depth (m)	Lab no.	Materials	$\delta^{13}C$ (per mil)	Conventional age	Calendar ages (cal a BP)	
						(a BP)	Intercept	Range (1σ)
	J7S06	15	Q200216	*Arca subcrenata*	–	5,350 ± 25	5,820	5,767–~5,884
	J7S03	15.07	542793	Oyster fragments	1.2	5,450 ± 30	5,940	5,885–~5,985
	J7S04	15.12	542794	Organic matters	−19.7	13,670 ± 40	16,480	16,359–~16,579
	J7S05	25.9	542795	Shell fragments	−6.4	32,270 ± 190	35,870	35,653–~36,105
JSWZK08	J8S04	16.22	Q200212	Oyster fragments	—	5,465 ± 30	5,955	5,891–~5,998
	J8S01	16.45	542796	Oyster fragments	−2.1	5,620 ± 30	6,135	6,064–~6,204
	J8S05	17.46	Q200214	Oyster fragments	—	5,225 ± 25	5,680	5,619–5,729
	J8S02	17.91	542797	Oyster fragments	−2.4	5,490 ± 30	5,980	5,906–~6,034
	J8S03	31.59	542798	*Potamocorbula ustulata*	−3.3	>43,500		
JSWZK09	J9S08	4.68	Q200766	*Potamocorbula laevis*	—	8,080 ± 40	8,675	8,578–~8,756
	J9S06	11.57	Q200210	Gastropod fragment	—	36,050 ± 420	40,365	39,893–~40,859
	J9S07	12.35	Q200207	*Nassarius variciferus*	—	32,580 ± 280	36,165	35,840–~36,455
	J9S01	16.96	542799	Oyster fragments	−8.0	>43,500		
	J9S02	18.58	542800	Gastropod fragment	−2.7	>43,500		
	J9S03	19.08	542801	Bivalve fragment	−1.1	>43,500		
	J9S04	19.23	542802	Organic matters	−18.1	34,280 ± 220	38,770	38,519–~38,981
	J9S05	24.93	542803	Bivalve fragment	−1.0	42,950 ± 620	45,900	45,300–~46,445
JSWZK10	J10S05	3.96	Q200961	Organic sediment	—	5,425 ± 45	6,235	6,206–~6,284
	J10S01	7.58	542804	*Barbatia bistrigata*	−1.3	6,170 ± 30	6,725	6,658–~6,778
	J10S02	11.2	542805	Corbicula fluminea	−10.3	>43,500		
	J10S03	24.3	542806	Gastropod fragment	−2.6	41,470 ± 500	44,645	44,205–~45,129
JSWZK11	J11S01	1.63	542790	*Pelecyora trigona*	−0.1	1,330 ± 30	980	924–~1,029
	J11S02	3.06	542791	Shell fragments	−0.4	1,290 ± 30	940	888–~993
	J11S06	11.42	Q200213	*Pelecyora trigona*	—	3,500 ± 20	3,495	3,442–~3,551
	J11S03	12.95	542792	*Oliva mustelina*	−1.0	7,050 ± 30	7,620	7,573–~7,657
	J11S04	15.92	542793	Shell fragments	−0.3	8,140 ± 30	8,770	8,659–~8,859
	J11S05	25.05	542794	Shell fragments	−13.0	>43,500		

*The lab numbers with Q as the prefix were the laboratory numbers of the Pilot National Laboratory for Marine Science and Technology (Qingdao), and the rest were from Beta Analytic (Miami).

10.3389/feart.2022.1107495

TABLE 3 OSL dates of 23 samples from the investigated boreholes.

Sample no.	Depth (m)	Core	Lab no.	U (μg/g)	Th (μg/g)	K (%)	Mass water content (%)	Dose rate (Gy)	Age (Ka)	Deviation (Ka)
JSW01	20.35	JSWZK01	2018A123	1.07	5.91	1.91	23.94	154.9	62.2	5.9
JSW02	26.65	JSWZK01	2018A124	1.19	5.61	1.89	7.45	320.7	113.8	11.4
JSW03	13.95	JSWZK03	2018A125	1.21	6.16	1.88	20.77	19.9	7.9	.3
JSW04	18.35	JSWZK03	2018A126	1.19	6.08	1.93	25.65	30.6	12.5	3.9
JSW05	30.7	JSWZK03	2018A127	1.19	5.81	1.97	9.24	270	94.5	4.8
JSW06	45.95	JSWZK03	2018A128	1.25	6.57	2.01	12.03	>400	>137.3	
JSW07	48.9	JSWZK03	2018A129	1.24	6.59	2.08	9.62	>400	>134.2	
JSW08	53.53	JSWZK03	2018A130	1.14	6.04	1.84	11.50	>400	>150.3	
JSW09	56.75	JSWZK03	2018A131	1.18	5.98	1.83	18.39	>400	>170.0	
JSW10	21.25	JSWZK04	2018A132	1.10	6.64	2.14	10.15	247.7	82.3	7.5
JSW11	30.75	JSWZK04	2018A133	1.18	5.65	2.06	10.55	270.2	94.1	10.5
JSW12	34.3	JSWZK04	2018A134	1.26	5.46	1.86	12.78	259.3	99.2	14.3
JSW13	37.7	JSWZK04	2018A135	1.30	5.47	1.86	13.32	260	97.1	17.1
JSW14	20.67	JSWZK05	2018A136	1.25	5.47	2.16	9.02	320.1	105.9	10.1
JSW15	27.75	JSWZK05	2018A137	1.22	6.47	2.10	13.96	>400	>166	
OSL-23	14.55	JSWZK07	2020A035	2.38	6.93	1.94	12	10.37	3.3	.2
OSL-24	21.15	JSWZK07	2020A036	2.14	8.68	1.94	24	84.14	31.0	5.6
OSL-25	24.1	JSWZK07	2020A037	2.17	5.40	1.89	17	99.49	36.8	5.4
OSL-26	26.3	JSWZK07	2020A038	2.08	7.33	1.98	19	111.63	39.4	7.1
OSL-27	30.5	JSWZK07	2020A039	3.10	8.80	1.89	21	219.43	71.4	7.3
OSL-28	1.85	JSWZK10	2020A040	2.02	7.94	2.17	19.5	3.65	1.2	.3
OSL-29	14	JSWZK10	2020A041	1.91	6.71	1.63	33	55.49	28.3	7.8
OSL-30	22.1	JSWZK10	2020A042	1.82	6.83	1.62	23.5	169.21	74.7	3.0

coastal, deltaic, subtidal, and shallow sea deposits). Individual facies associations were differentiated on the basis of sedimentological and fossil features, reflecting changes in depth, salinity, and degree of confinement. Diagnostic grain size characteristics for facies identification are summarized in Table 4. Depositional systems and their component facies are described from updip to downdip locations.

4.2.1 Alluvial deposits

Three facies (river channel, floodplain, and lacustrine bog) were recognized within alluvial deposits. These facies are described in detail as follows.

4.2.1.1 Facies I: River channel

This facies, commonly 3–10 m thick, is dominated by light gray fine-medium sand and gray coarse silt, with an overall fining upward trend (Figure 3A). The facies has a mean grain size (*Mz*) of 2.72–5.93 Φ with a sand proportion of 11%–83%, locally as high as 90%. Sorting is moderate to poor with a standard deviation (*SD*) of .85–1.55 Φ. The grain size frequency curve generally shows a unimodal distribution with a narrow peak (2–4 Φ of peak value) (Table 4). The grain size accumulation curve commonly exhibits a two-tier mode (Figure 4A). The saltating component dominates the curve with a proportion of >70%. Black organic mottles and calcareous concretions were occasionally found in some layers. No obvious marine fossils were found, except for some severely abraded shell fragments occasionally presenting in this facies. This facies generally has a sharp or erosional boundary with the underlying depositional units, typically representing a floodplain.

Thick sand bodies with lower erosional boundaries, an overall fining upward trend, and a lack of marine fossils are the characteristic features of fluvial deposits (Galloway and Hobday, 1983; Miall, 1992; Hori et al., 2001). Both the frequency and accumulation curves of this facies reveal a high-energy and steady single flowing-direction water environment (Folk and Ward, 1957). Accordingly, we interpret this facies as formed in laterally accreting river channels. Two AMS ^{14}C ages and eight reliable OSL ages ranged from 12,955 cal a BP to 106 ± 10 ka BP. These ages mostly fall within marine isotope stages 2 and 4. This facies, thus, seems to have been deposited through multiple cycles of fluvial activity during the Late Pleistocene.

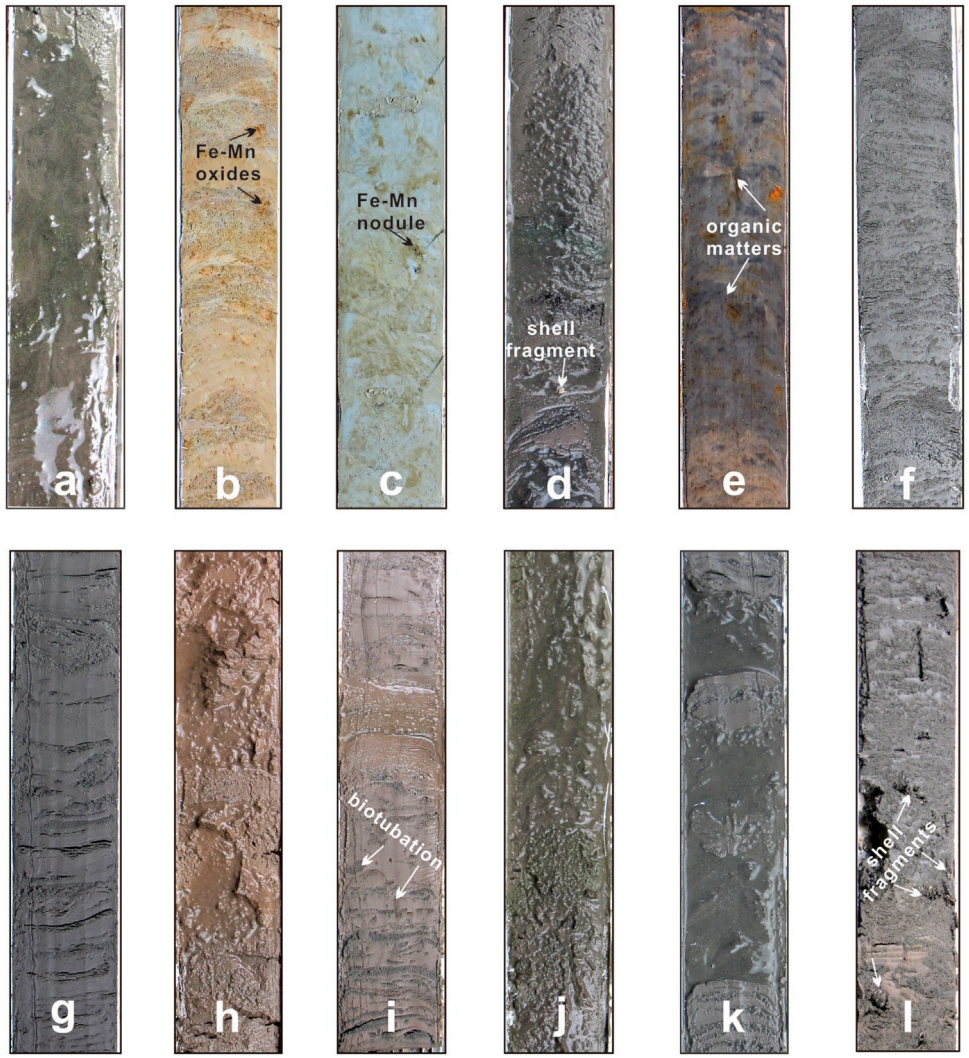

FIGURE 3
Representative photographs of facies in the Jiangsu coastal plain and radial tidal sand ridges. **(A)** River channel (depth 18.7–19.16 m) in the core JSWZK02; **(B)** floodplain (depth 13.4–13.87 m) in the core JSWZK05; **(C)** lacustrine bog (depth 59–59.4 m) in the core JSWZK03; **(D)** tidal river channel (depth 31–31.4 m) in the core JSWZK01; **(E)** supratidal flat (depth 1.8–2.2 m) in the core JSWZK01; **(F)** tidal flat (depth 9.7–10.1 m) in the core JSWZK05; **(G)** lagoon (depth 9.6–10 m) in the core JSWZK01; **(H)** delta front (depth 18.7–19.1 m) in the core JSWZK02; **(I)** prodelta (depth 11.8–12.2 m) in the core JSWZK08; **(J)** tidal sand ridge (depth 13.4–13.8 m) in the core JSWZK05; **(K)** tidal sand flank (depth 20.9–21.3 m) in the core JSWZK03; and **(L)** offshore (depth 7.4–7.8 m) in the core JSWZK10. All column lengths are 40 cm.

4.2.1.2 Facies II: Floodplain

This facies, generally 2–6 m thick, consists of gray to grayish-yellow silty clay and silt, locally interbedded with sandy silt layers (Figure 3B). The mean grain size ranges between 3.58 Φ and 7.71 Φ with poor to very poor sorting (SD: 1.07–2.65). Sand, silt, and clay contents are <10%, 24.2%–82.8%, and 2.65%–40.9%, respectively (Table 4). The grain size frequency curve principally outlines a unimodal-tailed distribution with a wide peak (4.5–6.5 Φ of peak value). The grain size accumulation curve commonly displays a two-tier mode (Figure 4B). The suspension component dominates the curve with a proportion of >80%. This facies generally contains plant material, iron manganese oxides, and calcareous concretions in some layers.

Scattered iron manganese oxides and calcareous concretions are good indicators of pedogenic processes in a subaerial terrestrial environment (Galloway and Hobday, 1983; Tanabe et al., 2006). Both the frequency and accumulation curves indicate a low-energy environment with gradually waning flows (Mycielska-Dowgiałło and Ludwikowska-Kędzia, 2011). Based on the aforementioned features, this fine-grained, poorly sorted facies is interpreted to represent a well-drained floodplain environment (Miall, 1992). No chronological data are available from this facies. However, as this unit is generally sandwiched between two river channel sediment bodies (i.e., facies I), it is likely that this facies may also be assigned to MIS 4 and 2.

4.2.1.3 Facies III: Lacustrine bog

This facies is dominated by steel gray to dark gray silty clay and clayey silt, partly interbedded with silt layers (Figure 3C). The thickness range is commonly 2–4 m. The mean grain size ranges from 5.8 to 7.1 Φ, with poor to very poor sorting (SD: 1.48–2.26). Sand, silt, and clay contents are .99%–12.14%, 68.77%–79.71%, and 14.38%–27.83%, respectively (Table 4). The grain size frequency curve

TABLE 4 Summary of grain size characteristics of facies associations.

Facies association	Mean grain size (Φ)	Sorting	Sand content (%)	Silt content (%)	Clay content (%)	Frequency curve	Accumulation curve
River channel	2.72–5.93	.85–1.55	11.09–83.01	7.24–75.7	.8–16.59	Unimodal distribution with a narrow peak (2–4 Φ of peak value)	Two-tier mode, saltating component dominating
Floodplain	3.58–7.71	1.07–2.65	1.86–68.93	24.22–82.78	2.59–40.97	Unimodal-tailed distribution with a wide peak (4.5–6.5 Φ of peak value)	Two-tier mode, suspension component dominating
Lacustrine bog	5.8–7.1	1.48–2.26	.99–12.14	68.77–79.71	14.38–27.83	Unimodal-tailed or bimodal-tailed distribution with a wide peak (4.5–7 Φ of peak value)	One-tier or two-tier mode, suspension component dominating
Tidal river channel	3.36–6.42	.77–1.76	7.5–78.49	18.7–74.2	1.42–21.33	Bimodal distribution with a coarse main peak (2.8–4.2 Φ of peak value) and a fine secondary peak (6–7.3 Φ of peak value)	Two-tier or three-tier mode, saltating component dominating
Supratidal flat	5.99–6.71	1.58–2.51	.66–5.24	76.47–81.19	13.82–21.3	Unimodal-tailed distribution with a wide peak (5–6 Φ of peak value)	Two-tier or three-tier mode, suspension component dominating
Tidal flat	4.56–6.88	.88–2.06	2.27–45.66	45.78–86.13	3.81–25.23	Bimodal distribution with a coarse main peak (4.3–5.1 Φ of peak value) and a fine secondary peak (7–8.2 Φ of peak value)	Two-tier or three-tier mode, saltating component dominating
Lagoon	4.39–6.82	1.17–2.25	.9–36.11	57.24–82.93	3.91–22.83	Bimodal or multimodal distribution with a wide peak (4.2–6.2 Φ of peak value)	Three-tier or multiple-tier mode, saltating component dominating
Delta front	4.28–6.17	.95–2.01	6.84–36.1	61.25–77.38	2.66–20.32	Bimodal distribution with a coarse main peak (3.8–5.2 Φ of peak value) and a fine secondary peak (6–7.5 Φ of peak value)	Two-tier or three-tier mode, saltating component dominating
Prodelta	4.79–7.25	1.18–2.06	.58–28.13	58.84–87.73	6.13–31.78	Unimodal-tailed distribution with a wide peak (4.2–7 Φ of peak value)	Two-tier or three-tier mode, suspension component dominating
Tidal sand ridge	2.23–5.27	.73–1.76	11.35–93.06	6.08–73.93	.71–20.34	Bimodal distribution with a coarse narrow peak (2–4.2 Φ of peak value) and a fine peak (6–7.5 Φ of peak value)	Three-tier mode, saltating component dominating
Tidal sand flank	3.6–7.02	.71–2.56	1.05–73.41	23.39–79.02	1.28–29.11	Unimodal-tailed distribution with a wide peak (4.2–6.5 Φ of peak value)	Two-tier or three-tier mode, saltating component dominating
Offshore	4.52–7.23	.99–2.27	1.14–65.12	25.8–78.61	2.66–29.74	Unimodal or bimodal distribution with a coarse main peak (4.3–5.1 Φ of peak value) and a fine secondary peak (7–8.2 Φ of peak value)	Two-tier or three-tier mode, suspension component dominating

mainly presents a unimodal-tailed or bimodal-tailed distribution with a very wide peak (4.5–7 Φ of peak value). The grain size accumulation curve commonly displays a one- or two-tier mode (Figure 4C). The suspension component dominates the curve with a proportion of >90%. Horizontal bedding and bioturbation are well displayed locally. Fe-Mn nodules and calcareous concretions were commonly found in the clay (Figure 3C). Some small freshwater gastropods, including *Radix* sp. and *Biomphalaria* sp., can be found in some beds.

Sediments in this facies invariably overlie with a sharp contact river–channel deposit, reflecting an abrupt channel abandonment (Amorosi et al., 2008). Horizontal bedding and bioturbation with very fine grain size reflect a low-energy sedimentary environment, consistent with grain size accumulation curves. Fe-Mn nodules and calcareous concretions commonly indicate the pedogenic processes in a terrestrial environment (Galloway and Hobday, 1983). Given the presence of a typical freshwater fauna, this facies is considered to have formed in a bog after channel abandonment (Hori et al., 2004). Like for floodplain deposits, neither AMS ^{14}C data nor OSL data are available from this facies.

4.2.2 Coastal deposits

Coastal deposits have been recognized in all study cores and can be subdivided into five facies referable to the tidal river channel, supratidal zone, tidal flat, and lagoon.

4.2.2.1 Facies IV: Tidal river channel

This facies, with a thickness of ~3–8 m, is mainly composed of gray fine sand and silt containing some marine and brackish water mollusk shells (Figure 3D), such as *Talonostrea* and *Corbicula fluminea*. The mean grain size ranges from 3.36 Φ to 6.42 Φ; the standard deviation (.77–1.76 Φ) indicates moderate to poor sorting. Sand, silt, and clay contents are 7.5%–78.49%, 18.7%–74.2%, and 1.42%–16.32%, respectively (Table 4). The grain size frequency curve mainly shows a bimodal distribution with a coarse main peak (2.8–4.2 Φ of peak value) and a fine secondary peak (6–7.3 Φ of peak value). The grain size accumulation curve commonly displays two- or three-tier modes (Figure 4D). Two saltation components dominate the curve with a total proportion of >90%. The fine saltation component generally has worse sorting but a higher content than the coarse

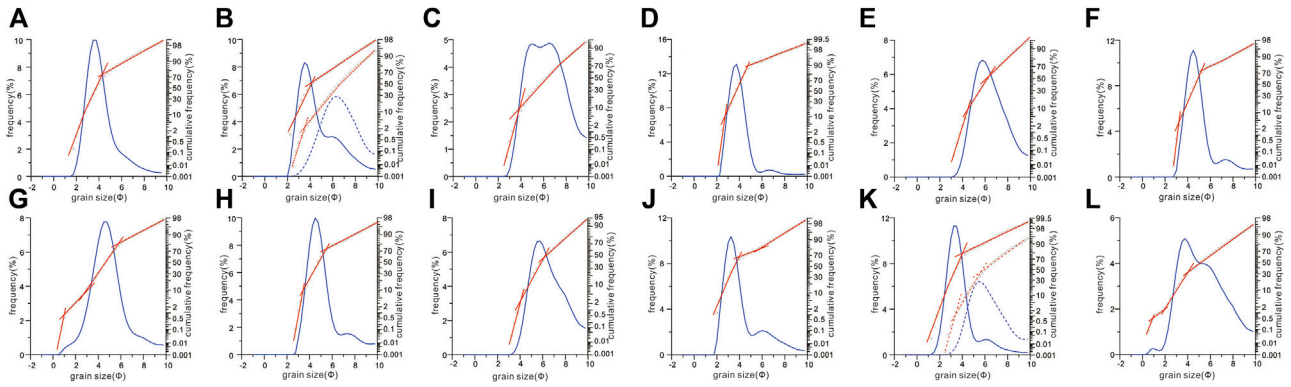

FIGURE 4
Grain size frequency (blue curve) and accumulation curves (red polyline) of typical sedimentary facies in the Jiangsu coastal plain and radial tidal sand ridges. **(A)** River channel at a depth of 25.55 m in the core JSWZK11; **(B)** floodplain at depths of 36.65 m (solid) and 40.75 m (dotted) in the core JSWZK04; **(C)** lacustrine bog at a depth of 15.35 m in the core JSWZK01; **(D)** tidal river channel at a depth of 26.45 m in the core JSWZK01; **(E)** supratidal flat at a depth of 1.75 m in the core JSWZK01; **(F)** tidal flat at a depth of 4.45 m in the core JSWZK02; **(G)** lagoon at a depth of 5.65 m in the core JSWZK01; **(H)** delta front at a depth of 1.25 m in the core JSWZK10; **(I)** prodelta at a depth of 4.25 m in the core JSWZK08; **(J)** tidal sand ridge at a depth of 16.35 m in the core JSWZK02; **(K)** tidal sand flank at depths of 20.55 m (solid) and 20.65 m (dotted) in the core JSWZK03; and **(L)** offshore at a depth of 7.45 m in the core JSWZK10.

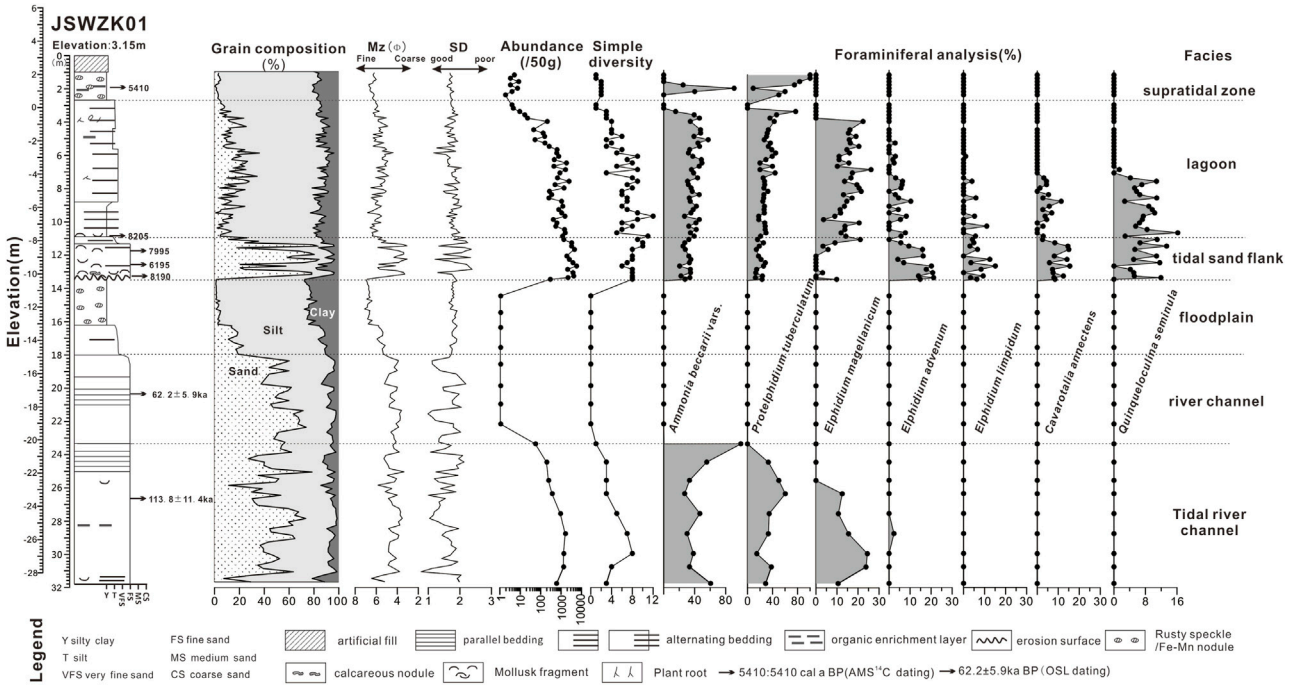

FIGURE 5
Comprehensive stratigraphic log of the core JSWZK01, showing lithology, grain size, and foraminiferal content. The borehole is divided into six sedimentary facies from the late Pleistocene tidal river channel and floodplain to the Holocene tidal sand flank, lagoon, and supratidal zone. It is to be note that the foramiferal data (i.e., abundance) changed abruptly at depths of 23.3 m and 13.4 m, indicating the end of Late Pleistocene marine transgression and the initiation of Holocene aggression in the core JSWZK01, relatively. For more detailed foraminiferal data, see Supplementary Table S1 in the attachment.

saltation component (Figure 4D). Average foraminiferal abundance and simple diversity in this facies (core JSWZK01) are 419 and 4, respectively. Benthic foraminifers are dominated by euryhaline taxa, such as *Ammonia beccarii* varsus (average percentage: 46.6%), *Protelphidium tuberculatum* (32.7%), and *Elphidium magellanicum* (11.18%) (Figure 5).

This facies has similar lithologic characteristics as the river channel facies, being characterized by well-sorted sandy deposits. However, the presence of mollusk shells and of a few euryhaline foraminifers indicates that these deposits accumulated in a brackish environment (Hori et al., 2001; Hori et al., 2004; Tanabe et al., 2006). The grain size frequency curve and accumulation curve are

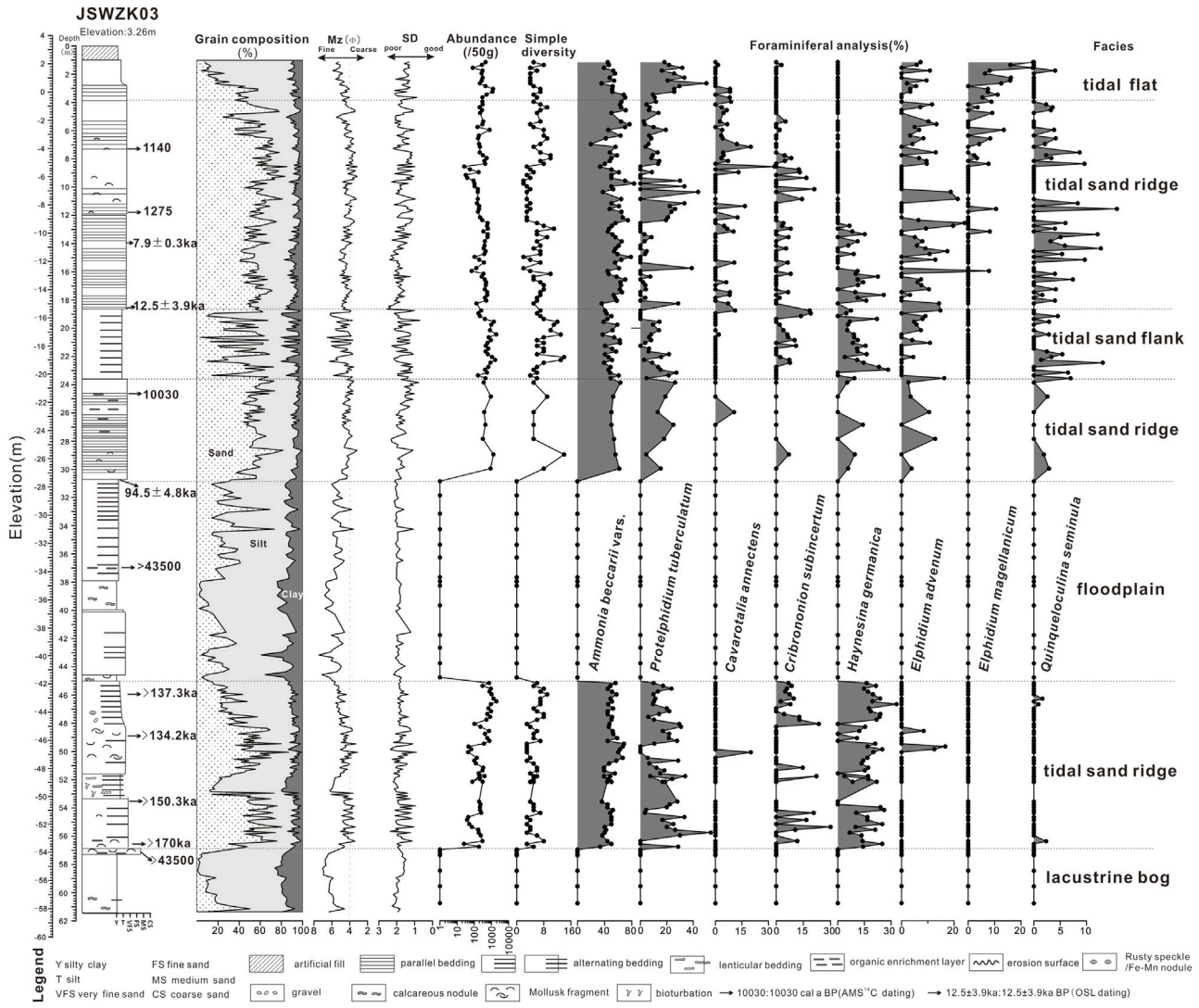

FIGURE 6
Comprehensive stratigraphic log of the core JSWZK03, showing lithology, grain size, and foraminiferal content. The borehole is divided into five sedimentary facies from the Late Pleistocene lacustrine bog, tidal sand ridge, and floodplain to the Holocene tidal sand ridge, tidal sand flank, and tidal flat. It is to be noted that the OSL ages are older than 130 ka BP below the depth of 45 m, indicating an age-unconstrained strata in this borehole. For more detailed foraminiferal data, see Supplementary Table S2 in the attachment.

also different from those of the river channel facies, which commonly miss the fine secondary peak and the fine saltation component (Figures 4A, D). Thus, this facies association is interpreted to reflect a tidal river channel that was intermittently influenced by tidal currents. A few AMS ^{14}C and OSL data in cores JSWZK01 and JSWZK07 reveal two stages of development for this facies, namely, ~30–40 ka BP and ~100 ka BP, which approximately correspond to stages MIS 3 and 5, respectively.

4.2.2.2 Facies V: Supratidal flat

This facies association consists of brown to yellowish-gray silt, partly interbedded with gray clayey silt or silty clay, containing abundant plant roots and ferruginous nodules (Figure 3E). Organic material and peat are locally present. Freshwater and brackish shells are common, including *Radix swinhoei* and *Gyraulus albus*. The range of *Mz* is 5.99–6.71 Φ, and the standard deviation of 1.58–2.51 Φ indicates poor to very poor sorting. Sand, silt, and clay contents are .66%–5.24%, 76.47%–81.19%, and 13.82%–21.3%, respectively (Table 4). The grain size frequency curve mainly shows a unimodal-tailed distribution with a wide peak (5–6 Φ of peak value). The grain size accumulation curve commonly displays two- or three-tier modes (Figure 4E). The suspension component dominates the curve with a total proportion of >50%.

Ferruginous nodules suggest subaerial exposure and pedogenic modification (Liu et al., 2016). Abundant plant roots, organic materials, and brackish/freshwater mollusk shells are commonly found in coastal marsh environments, which are typically located in the upper tidal flat to the supratidal zone (Hori et al., 2004). The dominant suspension component with a unimodal-tailed distribution also reveals a low-energy environment with gradually waning flows, which is possible during the ebb and flood. Based on distinct grain sizes and fossil characteristics,

this facies is considered to have formed in a supratidal flat environment.

4.2.2.3 Facies VI: Tidal flat

This facies consists of alternating gray to yellowish-gray silt with gray clayey silt or silty clay (Figure 3F). Wavy bedding and lenticular bedding are clearly recognized, whereas bioturbation and iron oxides are occasionally found. The mean grain size of this facies ranges from 4.56 Φ to 6.88 Φ with .88–2.06 Φ of standard deviation, indicating moderate to poor sorting. Sand, silt, and clay contents are 2.27%–45.66%, 45.78%–86.13%, and 3.81%–25.23%, respectively (Table 4). The grain size frequency curve and accumulation curves are similar to those of the tidal river facies association, with a bimodal distribution with a coarse main peak (4.3–5.1 Φ of peak value) and a fine secondary peak (7–8.2 Φ of peak value) in the frequency curve (Figure 3F). The grain size accumulation curve also displays two- or three-tier modes. The two saltation components dominate the curve with a total proportion of >80%. The fine saltation component has poorer sorting but a higher content than the coarse saltation component. The average foraminiferal abundance and simple diversity of this facies are 273 and 6 in the core JSWZK03, respectively. Similar to tidal river deposits, this facies is dominated by euryhaline foraminifera, such as *A. beccarii* vars (46.9%), *P. tuberculatum* (26.7%), and *E. magellanicum* (16.2%) (Figure 6).

Wavy bedding and lenticular bedding are reliable indicators of tidal processes (Galloway and Hobday, 1983). The grain size frequency and accumulation curves reveal a low-energy, multi-sourced, or bimodal current environment (Wang and Ke, 1997). The foraminiferal assemblage indicates the transition from a marine to a brackish/freshwater environment. As a whole, this facies is interpreted as a tidal flat. According to several AMS ^{14}C and OSL dates from the study cores, the development of the tidal flat took place at least in three distinct stages, including MIS 3, the early Holocene, and modern times.

4.2.2.4 Facies VII:Lagoon

This facies is composed mainly of gray to dark gray coarse silt alternating with gray silty clay (Figure 3G). The range of *Mz* is 4.39–6.82 Φ, and the standard deviation is 1.17–2.25 Φ, thus indicating poor to very poor sorting. The sand, silt, and clay contents are .9%–36.11%, 57.24%–82.93%, and 3.91%–22.83%, respectively (Table 4). The grain size frequency curve mainly shows bimodal or multimodal distributions with a wide peak (4.2–6.2 Φ of peak value). The grain size accumulation curve commonly displays three-tier or multiple-tier modes (Figure 4G). The two saltation components dominate the curve with a total proportion of >70%. Tiny marine shells or fragments are commonly found, including *Potamocorbula laevis*, *Umbonium thomasi,* and *Mactra veneriformis*. The average abundance and simple diversity in core JSWZK01 are 319 and 6, respectively. The dominant foraminiferal species are *A. beccarii* vars (37.1%), *P. tuberculatum* (30.2%), and *E. magellanicum* (13.18%) (Figure 5).

The rhythmical alternation of silt clay layers and the foraminiferal assemblage in this facies association are characteristic features of tidal flat deposits. However, frequency and accumulative curves are clearly distinct between lagoon and tidal flat facies (Figure 4; Wang Y. Z. et al., 2012). In addition, the brackish-dominated macrofaunal assemblage, some plant roots, and the small size of marine fossils indicate a high-salinity, barred marine environment, such as a lagoon (Como and Magni, 2009). Consistent with stratigraphic relations with underlying tidal sandy deposits, this facies is interpreted as having formed in a lagoon environment under conspicuous tidal influence. The lagoon likely evolved to a more restricted environment, as documented by the gradual decrease in abundance and simple diversity of foraminiferal assemblages from the bottom up in the core JSWZK01 (Figure 5). The AMS ^{14}C dates fall between 6,200 cal a BP and 5,410 cal a BP in the core JSWZK01, indicating that this facies association developed in a back-barrier environment at the onset of progradation of coastal barriers or delta systems during the middle Holocene (Li and Wang, 1991).

4.2.3 Deltaic deposits

Deltaic deposits were mostly recognized in cores from the NW part of our study area. Two distinct facies, namely, delta front and prodelta, were identified.

4.2.3.1 Facies VIII: Delta front

This facies is composed of gray coarse silt that in its lower part is interbedded with light gray fine sand and clayey silt (Figure 3H). It contains *Potamocorbula laevis*, *Talonostrea*, and *Mitrella bella*. No bioturbation was observed in the upper part of this facies. The range of *Mz* is 4.28–6.17 Φ, with a standard deviation of .95–2.01 Φ, indicating moderate to poor sorting. Sand, silt, and clay contents are 6.84%–36.1%, 61.25%–77.38%, and 2.66%–20.32%, respectively (Table 4). The grain size frequency curve mainly shows a bimodal distribution with a coarse main peak (3.8–5.2 Φ of peak value) and a fine secondary peak (6–7.5 Φ of peak value). The grain size accumulation curve commonly displays two- or three-tier modes (Figure 4H). The two saltation components dominate the curve with a total proportion of >80%. The fine saltation component has poorer sorting but a higher content than the coarse saltation component. The average benthic foraminiferal abundance is ~647, whereas simple diversity reaches ~18 in the core JSWZK07 (Figure 7). The dominant foraminiferal species are *A. beccarii* vars (36.7%), *A. pauciloculata* (14.8%), and *Nonionella decora* (10.2%) (Figure 7).

Relatively well-sorted coarse silt and the nearly absence of bioturbation in the upper part of this facies may reflect high-energy conditions and high sediment accumulation rates (Abrahim et al., 2008; Liu et al., 2009). Silt-sand alternations in the lower part of this facies and the bimodal distribution are inferred to reflect a combined hydrodynamic environment. Considering the euryhaline foraminiferal assemblage and stratigraphic relations with adjacent facies, this facies likely represents a delta front deposit (Galloway and Hobday, 1983), whereas its lower and upper parts represent distal to proximal sandy bars, respectively. The overall yellowish color in this facies suggests that the sediment source may have derived from the Yellow River (Cheng and Xue, 1997; Figure 3H). A few AMS ^{14}C and OSL dates from this facies fall between 3.3 ka BP and 145 cal a BP in the core JSWZK07.

4.2.3.2 Facies IX: Prodelta

This facies consists of gray to dark gray silty clay, alternating with light gray silt and fine sand layers or lenses. Lenticular bedding is common, and bioturbation is moderate (Figure 3I). This facies contains a few fragments of mollusk shells, such as *Arca subcrenata*, *Anomia chinensis*, *Dosinia biscocta, P. laevis,* and *Pelecyora trigona*. The mean grain size of this facies ranges from 4.79 Φ to 7.25 Φ, with a standard deviation of 1.18–2.06 Φ, indicating

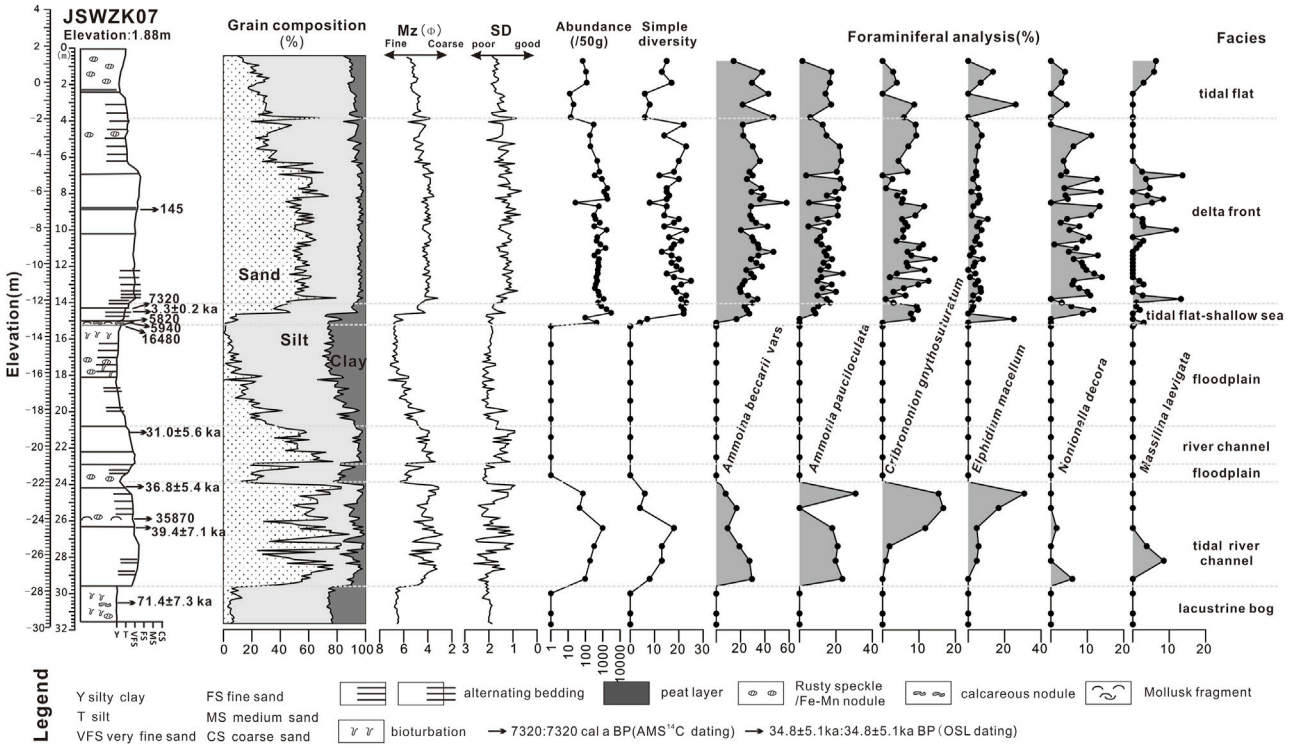

FIGURE 7
Comprehensive stratigraphic log of the core JSWZK07, showing lithology, grain size, and foraminiferal content. The borehole can be divided into six sedimentary facies from the Late Pleistocene lacustrine bog, tidal river channel, river channel, and floodplain to the Holocene tidal flat–shallow sea, delta front, and tidal flat. It is to be noted that the foramiferal data (i.e., abundance) changed abruptly at the depths of 24 m and 15.2 m, indicating the end of MIS 3 marine transgression and the initiation of Holocene aggression in the core JSWZK07, relatively. For more detailed foraminiferal data, see Supplementary Table S3 in the attachment.

poor to very poor sorting. Sand, silt, and clay contents are .58%–28.13%, 58.84%–87.73%, and 6.13%–31.78%, respectively (Table 4). The grain size frequency curve principally shows a unimodal-tailed distribution with a wide peak (4.2–7 Φ of peak value). The grain size accumulation curve commonly displays two- or three-tier modes (Figure 4I). The suspension component dominates the curve with a proportion of >50%.

The high proportion of suspended load, concurrently with a moderately abundant marine fossil assemblage and a moderate degree of bioturbation, is a reliable indicator of a low-energy, stressed marine depositional environment. This sedimentary environment was likely close to a fluvial mouth, such as a prodelta (Coleman and Wright, 1975). The overall brownish-yellow color (Figure 3I) may indicate direct sediment supply from the Yellow River (Cheng and Xue, 1997). This facies association developed during two distinct periods on the basis of a few chronological data, including MIS 3 and the late Holocene.

4.2.4 Subtidal deposits

Subtidal deposits are well exposed in seaward cores. They can be subdivided into two facies, namely, the tidal sand ridge and tidal sand flank.

4.2.4.1 Facies X: Tidal sand ridge

This facies is dominated by yellowish-gray to gray fine-medium sand and coarse silt (Figure 3J). *Mz* ranges from 2.23 to 5.27 Φ, and the contents of sand, silt, and clay are 11.35%–93.06%, 6.08%–73.93%, and .71%–20.34%, respectively. Sorting is moderate to poor. Like the tidal river facies, the grain size frequency curve mainly shows a bimodal distribution with a coarse, narrow peak (2–4.2 Φ of peak value) and a fine peak (6–7.5 Φ of peak value) (Figure 4J). The grain size accumulation curve commonly displays a three-tier mode. The two saltation components dominate the curve with a total proportion of >80% (Table 4). The fine saltation component generally has poorer sorting and a lower concentration than the coarse saltation component. Marine mollusk shells are scarce and mostly fragmented. In the core JSWZK03, the average foraminiferal abundance and simple diversity are ~333 and 6, respectively. Euryhaline *A. beccarii* vars (57.3%) and *P. tuberculatum* (10.1%) are the dominant foraminiferal species (Figure 6).

Relatively well-sorted coarse sediments and a few marine shell fragments are characteristic of a high-energy, marine-influenced environment. The bimodal distribution and three-tier mode with two saltation components of grain size curves are consistent with a to-and-fro movement in a tidally influenced environment. Although it is difficult to distinguish this facies from tidal river channel deposits on the basis of grain size analysis alone (Figures 4D, J), the fossil assemblages showed some marked differences. For example, the tidal channel river facies had some brackish shell fragments, such as *Corbicula fluminea*, which were only rarely found in this facies. This facies also had a higher diversity of foraminifers (4–10) than those of the tidal river channel (2–5) (see Figures 5, 6), indicating a subtidal

environment. Additionally, the grain size frequency curve of this facies commonly displays a bimodal distribution with a coarse narrow peak and a fine peak, which is similar to grain size characteristics of tidal sand ridges detailed by previous studies in the south Yellow Sea (Wang et al., 2019a). This facies, thus, is interpreted as having formed in a tidal sand ridge. Based on numerous AMS ^{14}C and OSL dates in cores JSWZK03, JSWZK04, and JSWZK05, tidal sand ridges developed at least during two distinct phases, namely, the early–middle Holocene and an age possibly older than MIS 5, although OSL data are not conclusive.

4.2.4.2 Facies XI: Tidal sand flank

This facies consists of light gray fine sand, alternating with gray to dark gray clayey silt and silt (Figure 3K). It contains a few fragments of mollusk shells, such as *Arca subcrenata* and *P. laevis*. The mean grain size of this facies ranges from 3.6 Φ to 7.02 Φ with a standard deviation of .71–2.56 Φ, indicating moderate to very poor sorting. The sand, silt, and clay contents are 1.05%–73.41%, 23.39%–79.02%, and 1.28%–29.11%, respectively (Table 4). The grain size frequency curve of sandy layers is similar to that of tidal sand ridges, whereas the curve of clayey silt principally shows a unimodal-tailed distribution with a wide peak (4.2–6.5 Φ of peak value). The grain size accumulation curve commonly displays two- or three-tier modes (Figure 4K). The suspension component dominates the curve with a proportion of >60% in the silty layer. The average foraminiferal abundance and simple diversity are ~716 and 8 in the core JSWZK03, respectively (Figure 6). Euryhaline *A. beccarii* vars (48.8%) and *Haynesina germanica* (10.1%) are the dominant foraminiferal species.

The lithological characteristics are quite similar to the "tidal inlet" facies of published boreholes 11DT03 and 11DT04 described by Ji et al. (2015) or the sand ridge bottom facies described by Yin et al. (2016). This facies shows characteristic sand–mud couplets, with obviously contrasting grain size characteristics (see Figure 4K). This facies exhibits a lateral transition to tidal sand ridge deposits and shows intermediate characteristics between the tidal sand ridge and offshore facies in terms of grain size and foraminiferal abundance. Thus, it is inferred to represent a slightly deeper and lower-energy (subtidal) environment than tidal sand ridges, which we interpret as a tidal sand flank.

4.2.5 Shallow sea deposits

4.2.5.1 Facies XII: Offshore

This facies is dominated by dark gray clayey silt and silty clay, locally interbedded with lenses of gray coarse silt and fine sand (Figure 3L). It has an *Mz* range of 4.52–7.23 Φ, with contents of sand, silt, and clay of 25.8%–78.61%, 2.66%–29.74%, and 1.14%–65.12%, respectively (Table 4). Sorting is poor to very poor. The grain size frequency curve mainly shows a unimodal or bimodal distribution with a coarse main peak (4.3–5.1 Φ of peak value) and a fine secondary peak (7–8.2 Φ of peak value). The grain size accumulation curve commonly displays two- or three-tier modes (Figure 4L). The suspension components dominate the curve, with a proportion of >50%.

Bioturbation is very common. Marine mollusk shells are abundant and include *Arca subcrenata*, *Mactra veneriformis*, *Potamocorbula laevis*, *Talonostrea,* and *Anomia* sp. The average foraminiferal abundance of this facies has the highest value (~1,645 per 50 g of dry sediment) of the whole succession. The average simple diversity is also the highest, up to 25. The dominant foraminiferal species are *A. beccarii* vars (24.8%), *Cribrononion gnythosuturatum* (10.3%), *Nonionella decora* (8.2%), and *A. pauciloculata* (6.8%) (Figure 7).

The abundance of marine shells and bioturbation, the high diversity, and abundance of foraminifers with high concentrations of relatively stenohaline species coupled with a predominant fine-grained sediment and a dominant suspension component indicate a low-energy offshore environment (He et al., 2018; 2019). The development of this facies association took place at least during two distinct periods, including MIS 3 and the mid-late Holocene, respectively.

4.3 Late Pleistocene to Holocene stratigraphic architecture of the Jiangsu coastal plain and tidal sand ridge area

To reconstruct the Late Pleistocene to Holocene facies architecture in the Jiangsu coastal plain and tidal sand ridge area, we performed stratigraphic correlation among the 10 cores investigated in this study and eight cores from previously published studies (see Figure 1C). The stratigraphy of the study area was depicted through two SW–NE (along-dip)-oriented stratigraphic transects (Figures 8, 9), transversal to the modern coastline, and a NW–SE (along-strike)-oriented transect (Figure 10), parallel to the modern coastline.

4.3.1 Along-dip transects

4.3.1.1 Transect X-X′

This transect (Figure 1C) is located in the northern part of the Jiangsu coastal area. From proximal to distal locations, it includes cores JSWZK07, JSWZK08, JSWZK10, 07SR03, and JSWZK11 (Figure 8, core 07SR03 modified from Zhang et al., 2014).

Two major intervals with marine or mixed marine-coastal deposits represent a prominent feature across the whole transect. Marine and coastal deposits are invariably separated from underlying laterally continuous alluvial units by distinctive transgressive surfaces (Figure 8). The marine influence is highest at or a few meters above the transgressive surfaces, where shallow marine deposits are dominant. Offshore clays are generally overlain by prograding deltaic or subtidal sandy complexes. There is also clear distal to proximal transition from thick tidal sand ridge and shallow sea sediments in the NE to deltaic and tidal river channel facies in a more SW position. A large number of AMS ^{14}C and OSL dates assign the uppermost marine interval (tidal flat and shallow marine sediments) to the early Holocene, suggesting that marine ingression in the current tidal sand ridge area occurred before 8,800 cal a BP. According to the available radiocarbon dates and based on the morphological evolution of the study area, the overlying, prograding delta complex is thought to be the old Yellow River Delta of northern Jiangsu during the period in which the Yellow River captured the Huaihe River in 1128–1855 AD (Xue et al., 2010; Liu et al., 2013).

Unlike the Holocene marine interval, the older one is made up predominantly of tidal river channels and deltaic deposits, testifying to a more complex fluvial–marine interaction. The age of this older marine deposit is centered around 35–38 ka BP, with a few data ranging between 28 and 39 ka BP (Figure 8). This suggests an age attribution to the MIS 3 period. Clearly, deltaic progradation during MIS 3 occurred more seaward than Holocene progradation, which is consistent with the significantly lower eustatic rise during MIS 3.

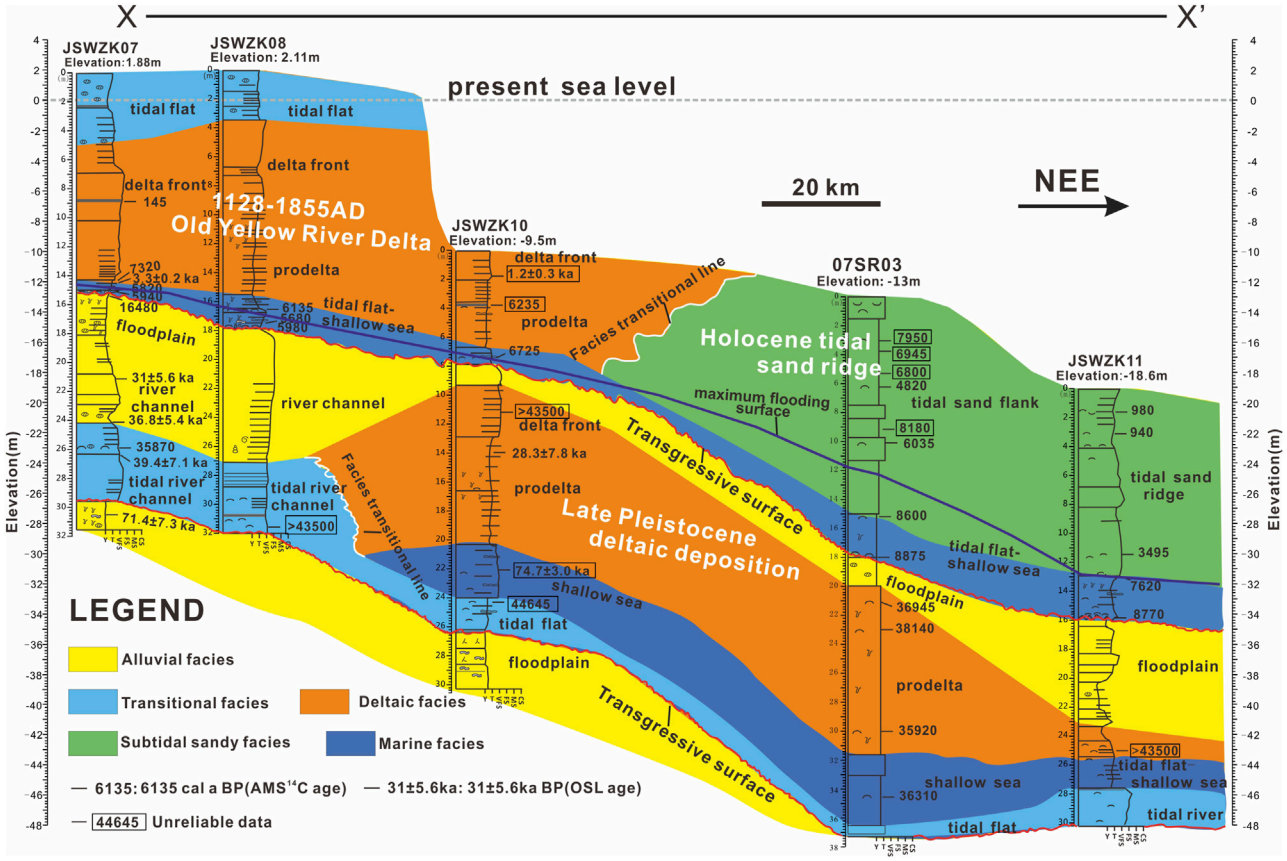

FIGURE 8
Facies architecture along coastal transect X-X′. The core 07SR03 is modified from Zhang et al. (2014).

4.3.1.2 Transect Y-Y′

This transect is located in the south of the Jiangsu coastal plain and partly across the shelf tidal sand ridge area, about 60 km south of transect X-X′. From proximal to distal locations, this transect includes cores JSWZK01, JSWZK02, JSWZK03, Y1, Y2, JSWZK04, and JSWZK05 (Figure 9, cores Y1 and Y2 are modified from Wang et al. (2015) and Yin et al. (2016), respectively).

The stratigraphy reconstructed from seven boreholes displays striking similarities with the facies architecture illustrated along transect X-X′; two major intervals of marine sedimentation, bounded by prominent transgressive surfaces, are separated by a thicker alluvial unit (Figure 9). Along transect Y-Y′, marine sediments consist entirely of tidal sand ridge facies at seaward locations, whereas the landward areas are dominated by coastal facies, including lagoon and tidal river channel deposits (Figure 9).

A large number of radiocarbon dates from transect Y-Y′ reveal that the uppermost marine interval, about 10–30 m thick, is of Holocene age. Sedimentary facies in the westernmost core JSWZK01 are composed of tidal sand bar and lagoon facies that gradually transition seaward to tidal sand ridge and tidal sand flank facies (Figure 9). Multiple dating along this transect suggests that the sea may have reached the current sand ridge region around 9,000 cal a BP (see core JSWZK05 in Figure 9).

The older marine deposits are mainly tidal sand ridge and tidal sand flank facies in landward transition to tidal river channel deposits. Several AMS ^{14}C dates from this marine interval yielded ages older than 40,000 a BP, which may not be reliable due to the limit of carbon-14 dating. In contrast, a few OSL dates cluster around 110–170 ka BP (though they may exceed 130 ka BP locally—Figure 9), suggesting that the older marine interval may have formed during MIS 5.

Alluvial deposits between these two marine intervals are mostly river channel and floodplain facies and yielded ages ranging between 20,000 and 90,000 a BP, suggesting deposition between MIS 2 and MIS 4. Unlike section X-X′, MIS 3 deposits were not encountered in transect Y-Y′, which may imply that they originally were relatively thin or that they were eroded by subsequent fluvial activity.

4.3.2 Along-strike transect

4.3.2.1 Transect Z-Z′

This transect runs along strike, parallel to the present coastline of the northern Jiangsu coastal plain, including cores JSWZK09, JSWZK10, 07SR01, JSWZK03, NTCJ3, JC-1203, Sanming, and 07SR11 from north to south, respectively (Figure 10, cores 07SR01, NTCJ3, JC-1203, Sanming, and 07SR11 modified from Yin and Zhang (2010), Wang Y. et al. (2012), Zhang X. et al. (2013), Sun et al. (2015), and Xiao (2015), respectively).

Similar to the along-dip transects, two intervals of marine or coastal-marine sedimentation and two intervals of alluvial deposits can be found in most cores along this transect. The uppermost marine interval in this transect mainly consists of Holocene tidal sand ridges that gradually turn into deltaic sediments from south to north. A few radiocarbon dates reveal that deltaic deposits were the subaqueous

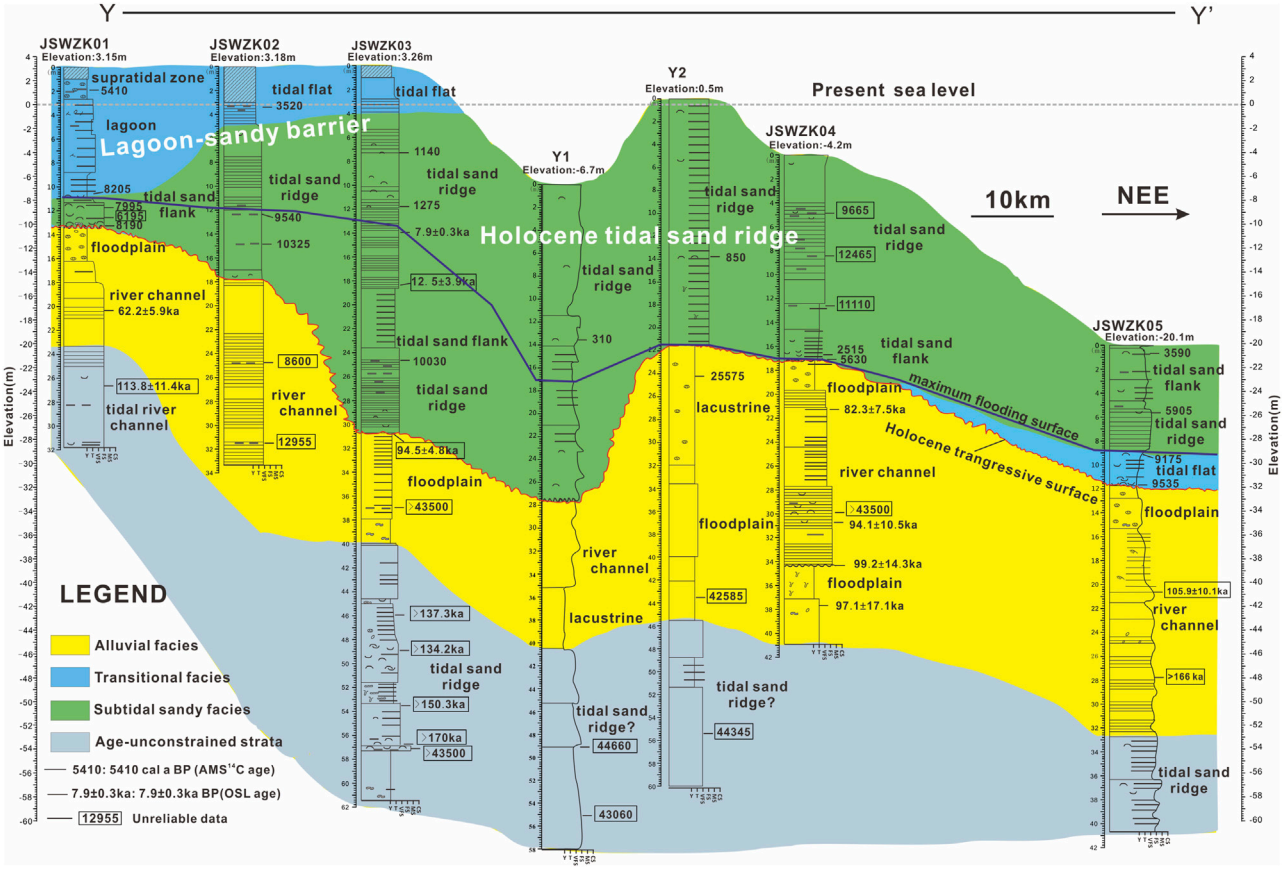

FIGURE 9
Facies architecture along coastal transect Y-Y′. Cores Y1 and Y2 are modified from Wang et al. (2015) and Yin et al. (2016), respectively.

delta part of the old Yellow River Delta between 1128 and 1855 AD in Jiangsu Province. The tidal sand ridge seems to have formed earlier than 4,800 cal a BP near the present coastline (see Figure 10).

Older (Late Pleistocene) marine or coastal-marine deposits in transect Z-Z′ are (i) suspected tidal sand ridge and tidal sand flank facies in the southern part of the study area, likely assigned to MIS 5, and (ii) deltaic deposits in the north, attributed to MIS 3. The ~30-m-long boreholes in the northern side may be too short to unravel MIS 5 deposits. On the other hand, transgressive MIS 3 deposits in the south are missing. The southernmost core (07SR11) lacks Holocene tidal sand ridge/sand flat facies, which are replaced by thicker tidal flat to shallow marine deposits, indicating the limit of tidal sandy influence.

5 Discussion

5.1 Changes in sedimentation rates and Holocene radial tidal sand ridge development

The formation of the RTSR in this area has been widely discussed by several studies (Li and Zhao, 1995; Li et al., 2001; Wang Y. et al., 2012; Yin et al., 2016). A consensus has been reached that a convergent–divergent tidal current field and large amounts of sediment are prerequisites for the formation of the RTSR (Zhu, 1998). Thus, the initiation of the convergent–divergent tidal current field and periods of high sediment flux appear to be critical to understanding the evolution of the RTSR.

According to simulations of regional paleotidal currents since the Holocene (Wang et al., 1998), the convergent and divergent tidal current fields in the study area were established between 10 and 8.5 ka BP, which implies that the RTSR could develop in the coastal area of Jiangsu Province after 10 ka BP. Zhu and Chang (2001) generally agreed with this opinion; however, they considered the early Holocene RTSR smaller than the present one due to reduced sediment supply during the early Holocene. Based on the evolution history of large rivers flowing to the SYS and a few ancient charts in the study area (Zhang, 1988), Liu and Xia (2004) proposed that the present RTSR could have formed since 2 ka BP and that it developed rapidly in response to the southward migration and supply of a large amount of sediment by the Yellow River after 1128 AD. Strong tidal currents could have shaped the radial morphology of the RTSR after the Yellow River flowed northward to the Bohai Sea since 1855 AD. Yin et al. (2016) concluded likewise that the formation of tidal sand ridges was highly related to remarkable sand input from the old Yellow River Delta after 1128 AD, as some radiocarbon ages from their cores indicated the initiation of tidal ridges since 600 years ago.

On the basis of seismic profiles and core data from the subaqueous sand ridge field, Wang et al. (1998) hypothesized that the RTSR could have formed after the early Holocene transgression, like other

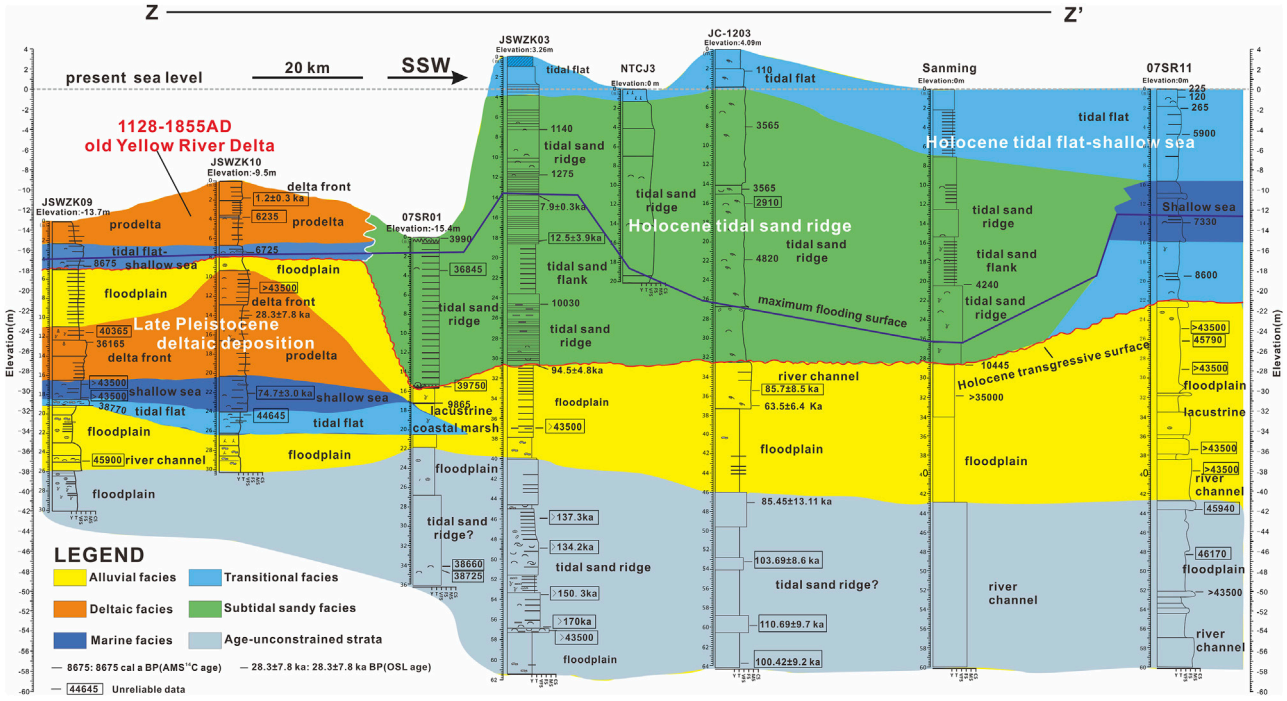

FIGURE 10
Facies architecture along coastal transect Z-Z′. Cores 07SR01, NTCJ3, JC-1203, Sanming, and 07SR11 are modified from Yin and Zhang (2010), Zhang X. et al. (2013), Xiao (2015), Wang Y. et al. (2012), and Sun et al. (2015), respectively.

Holocene sand ridges around the world (McBride and Moslow, 1991; Park et al., 2006). This hypothesis also agrees with simulations of regional paleotidal currents since the Holocene (Wang et al., 1998; Wang, 2002). Moreover, based on detailed sequence stratigraphic analysis of the SYS area since the MIS 5 period, Xia et al. (2012) delineated the relationship between relative sea-level change and the evolution of the RTSR, suggesting that the RTSR could start to develop after the submergence of the study area, following the early Holocene sea level jump around 9 cal ka BP.

However, contrary to the investigations of subaqueous sand ridges, studies from terrestrial tidally influenced sandy sediment attached to the present RTSR presented a different interpretion on the formation history of the Jiangsu coastal area (Figure 1C). Chen et al. (1995) recognized the terrestrial tidally influenced sandy sediment as the earliest sand ridges after detailed analysis of sedimentary facies, which were related to large sediment input from the Yangtze River around 7–6.5 ka BP, during the Holocene maximum transgression. Li et al. (2001) argued that the RTSR developed after 7.5 ka BP, prograding seaward under the Holocene normal regression. Chough et al. (2004) also considered that the RTSR off the Jiangsu Coast may represent "regressive," highstand deposits that formed when sea level reached the present position at about 6 ka BP.

In summary, contrasting opinions about the formation and evolution of the RTSR mainly focused on when and where the original sand ridges developed, and distinct views led to highly different reconstructions. In order to contribute new data to this debate, in this study, we applied to the Holocene RTSR a technique based on age–depth plots from previous work (Figure 11A), which has proved to be an effective method to figure out the complex sedimentary evolution of depositional systems under high sediment supply conditions (He et al., 2019). The initiation of the RTSR in the study area is defined by the oldest depositional age obtained from tidal flat deposits, namely, ~9,000 cal a BP (Figure 11A; Liu et al., 2013; Xue, 2014).

Using published chronological data from cores, we found that sedimentation rates are clearly distinct before and after ~800 cal a BP. In particular, sedimentation rates range between .37 mm/a and 3.3 mm/a during ~9,000–800 cal a BP, but they dramatically increase to 18.9–108.7 mm/a after ~800 cal a BP (Figure 11B). This abrupt increase in the sedimentation rate of tidal sand ridges strikingly coincides with the moment (1128–1855 AD) in which the Yellow River delivered sediments to the Yellow Sea, following the capture of the Huaihe River (Xue et al., 2010; Liu et al., 2013). Thus, the growth of the RTSR can be subdivided into two stages. The first stage of bedform migration, from ~9,000 cal a BP to 1128 AD, is characterized by generally slow deposition, with locally increasing sedimentation rates under highstand conditions (since 5,000–3,000 a BP). The second stage, after 1128 AD, is a period of rapid development, when the sand ridge field received a large amount of sediment from the Yellow River and rapidly built its modern shape. A significant development of the RTSR following maximum marine ingression, particularly during the latest Holocene, can be clearly observed in the stratigraphic cross sections of Figures 9, 10. According to the available data, no direct evidence was found for the renewed growth of the sand ridges after the Yellow River re-entered the Bohai Sea northward in 1855 AD.

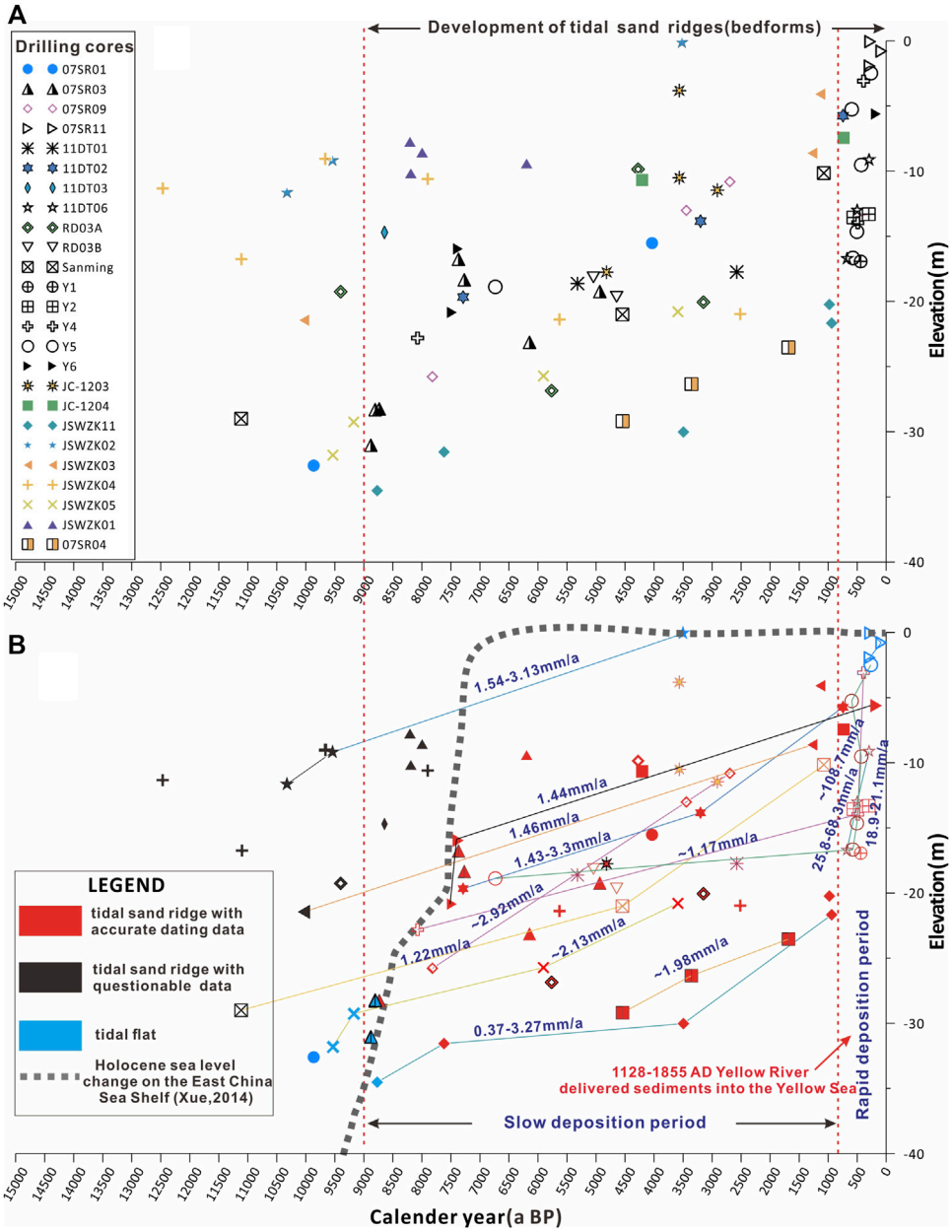

FIGURE 11
(A) Age–depth plot of collected drilling cores in the RTSR; **(B)** different sedimentary rates of the tidal sand ridge during 9,000 a BP–1128 AD and 1128–1855 AD.

5.2 Sedimentary evolution of the radial tidal sand ridge region since the Late Pleistocene

According to the stratigraphic analysis of 10 continuous cores and previous data (Figures 8–10), the study area documents a cyclic sedimentation pattern of alluvial and coastal/shallow marine deposits that define transgressive–regressive successions deposited over the last two interglacial–glacial cycles. Along-dip facies changes include a transition from fluvio-deltaic deposits in the northern part of the study area to tidally influenced sand deposits to the south.

5.2.1 MIS 5 and older periods (>100 ka BP)

Although results from OSL dating are not conclusive about its age, the sand tidal ridge facies assigned to the early MIS 5 (and possibly to older periods) is well preserved in the southern part of the study area (e.g., core JSWZK03) (Figures 9, 10). Previous numerical simulations have revealed that the formation and evolution of the tidal current system in the south Yellow Sea were mainly controlled by the interaction between the East China advancing tide wave and the position of the Jiangsu–Shandong paleocoastline, especially the Jiangsu paleocoastline (Wang et al., 1998; Uehara et al., 2002), as the bedrock coast of the Shandong Peninsula has basically kept steady

since the Early Cretaceous (Wang S. J. et al., 2009). The reconstruction of Pacific sea-level changes since the Late Pleistocene implies that the early MIS 5 sea-level position was comparable to the present position (Chappell et al., 1996). The sediment source for the MIS 5 RTSR likely was the paleo Yangtze River (Wang et al., 2007b; Wang Y. et al., 2012; Wang et al., 2019b).

No early MIS 5 deposits were encountered in the north because of insufficient borehole depth (Figures 8, 10). However, two ~70-m-long cores (SYS-0701 and SYS-0702) from the south Yellow Sea, adjacent to the northernmost part of the study area, at a water depth of ~33 m, revealed the presence of a MIS 5 nearshore to shallow marine facies (Liu et al., 2010). Neither prominent deltaic deposits nor tidal sand ridge facies were encountered in the northern area. Tidal river deposits assigned to the early MIS 5 were observed on the basis of individual (JSWZK01) core data.

5.2.2 Late MIS 5 and MIS 4 periods (~60–100 ka BP)

Terrestrial deposition, including riverine and floodplain environments, dominated the study area during the late MIS 5 and MIS 4. River channel facies made up of thick, homogeneous coarse sand bodies was recognized in most cores (e.g., JSWZK04, Figure 9). Severely abraded marine shell fragments locally floor erosion surfaces, indicating the widespread occurrence of condensed stratigraphic intervals and hiatal surfaces during this period (see core JSWZK04 in Figure 9). The sedimentary evolution of the study area was highly related to sea-level fluctuations during the Late Pleistocene in the Yellow Sea (Liu et al., 2010).

5.2.3 MIS 3 period (~24–60 ka BP)

Tidal flat and shallow marine deposits assigned to MIS 3 mark the onset of renewed (minor) transgression in the study area. These deposits are overlain by a characteristic prograding succession of deltaic deposits in northern cores (e.g., JSWZK09 and JSWZK10) (Figures 8, 10), whereas tidal river deposits can be found in landward cores (e.g., JSWZK07 and JSWZK08).

The existence of marine deposits assigned to MIS 3 on the Jiangsu Coast has been debated in previous studies. Sedimentological analysis of cores BY1, 07SR01, and Longgang indicates that marine-influenced environments likely existed during MIS 3 (e.g., Zhang et al., 2010; Xia et al., 2013; Xia and Zhang, 2018); this hypothesis is also supported by numerical modeling of the MIS 3 transgression along the Jiangsu and Fujian coasts (Ye et al., 2016; Yu et al., 2016). Conversely, nearby boreholes, such as cores 07SR09 and 07SR11 (Sun et al., 2014; 2015), showed that MIS 3 deposits are entirely of continental origin. Unfortunately, most chronologic attributions to MIS 3 lack supporting OSL dates or are mostly constrained by AMS ^{14}C ages ranging between 35,000 and 40,000 a BP, which is close to the dating limits and could be questionable (Yin and Zhang, 2010; Zhang et al., 2010; Xia et al., 2013; Sun et al., 2014; Sun et al., 2015; Xia and Zhang, 2018).

Marine deposits have been reported at −20–−50 m elevation around the present coastline on the basis of macro- and micro-fossil (foraminifers) analyses from cores JC-1204 and 07SR01 (Xia et al., 2013; Xiao, 2015). Liu et al. (2013) confirmed the presence of MIS 3 deltaic deposits from core SYS-0701 through OSL dating in the southern Yellow Sea. Gao et al. (2021) detailed a mass of post-infrared (IR) IR-stimulated luminescence (pIRIR) ages and found no MIS 3 marine deposits in the core JCP01 beyond the limit of Holocene marine ingression. Therefore, it thus appears to exist a marked correlation between the formation of MIS 3 marine deposits and the distance from the coastline.

Although dating of JSWZK10 deltaic deposits yielded two AMS ^{14}C ages >40 ka BP and two OSL results ranging between 28 ka and 75 ka BP, the adjacent core JSWZK07 provided consistent OSL results in tidally influenced strata (36.8 ± 5.4 ka BP and 39.4 ± 7.1 ka BP, respectively) (see Figures 7, 8). We considered these adjacent tidal and deltaic deposits as indicators of coeval MIS 3 sedimentation because of the same elevation (−20–−30 m) and short distance between them. Our findings support the presence of a large active delta during MIS 3, which had been recognized from a series of seismic profiles and core data in the south Yellow Sea (Liu et al., 2010). The delta likely formed between 40 ka BP and 28 ka BP in the late MIS 3. Progradation of the MIS 3 delta took place in a more seaward position relative to its Holocene counterpart (Figure 8), which is consistent with a lower relative sea-level position during this period (Chappell et al., 1996).

It is remarkable that almost no MIS 3 deltaic or marine sediments were found in the southern part of our study area (Figures 9, 10), though thin marine layers have been reported from cores 07SR09 and 07SR04 in adjacent areas (Sun et al., 2014; Sun et al., 2015). This could be related to a relatively weak MIS 3 marine transgression and/or later (MIS 2) intense fluvial erosion in the region.

5.2.4 MIS 2 and the early Holocene period (~9–24 cal ka BP)

The whole south Yellow sea shelf was mostly subaerially exposed when sea-level position retreated to the Okinawa trough during the Last Glacial Maximum and early Holocene (Li et al., 2014). At that time, terrestrial, riverine, and lacustrine environments dominated the study area. A ~2–4-m-thick stiff clay layer was found in several cores, such as JSWZK01 (13.4–16.2 m), JSWZK04 (17.18–19.68 m), JSWZK06 (10.4–12.3 m), and JSWZK07 (15.08–18.1 m) (Figures 9, 10), thus representing a laterally continuous marker bed for stratigraphic correlation in the southern Jiangsu Plain and in the Yangtze deltaic area (Li et al., 2001; Sun et al., 2015). This overconsolidated horizon represents a stratigraphic unconformity of worldwide significance; it corresponds to a weakly developed paleosol that formed at the MIS 3/2 transition in response to the last phase of sea-level fall (Amorosi et al., 2017), and it is likely correlative with the development of the adjacent Yangtze River incised-valley systems (Saito et al., 2001; Li et al., 2002).

5.2.5 9,000–7,000 cal a BP

Marine ingression occurred in the present RTSR field area during the early Holocene sea-level jump, around 9,000–8,500 cal a BP (Hori and Saito, 2007). This transgressive trend is documented by the presence of typical tidal flat facies in the seaward-most cores (i.e., core JSWZK05) (Figures 8, 9, 12A). Radial tidal sand ridges are supposed to have been formed during this period by numerous hydrodynamic model simulations (Wang et al., 1998; Zhu and Chang, 2001). Our detailed sedimentary facies analysis, corroborated by several radiometric dates, supports this hypothesis, indicating that tidal sand ridges were active since about 9,000 cal a BP.

With rapid relative sea-level rise, the shoreline reached its present position around 8,200–8,500 cal a BP (see the cores JSWZK01 and JSWZK09 in Figures 8, 10). In the northern region, tidal flat and shallow marine environments developed with no apparent influence of radial tidal currents. In contrast, tidal sand ridges (bedforms) migrated in the southern area. A coastal barrier–lagoon system was

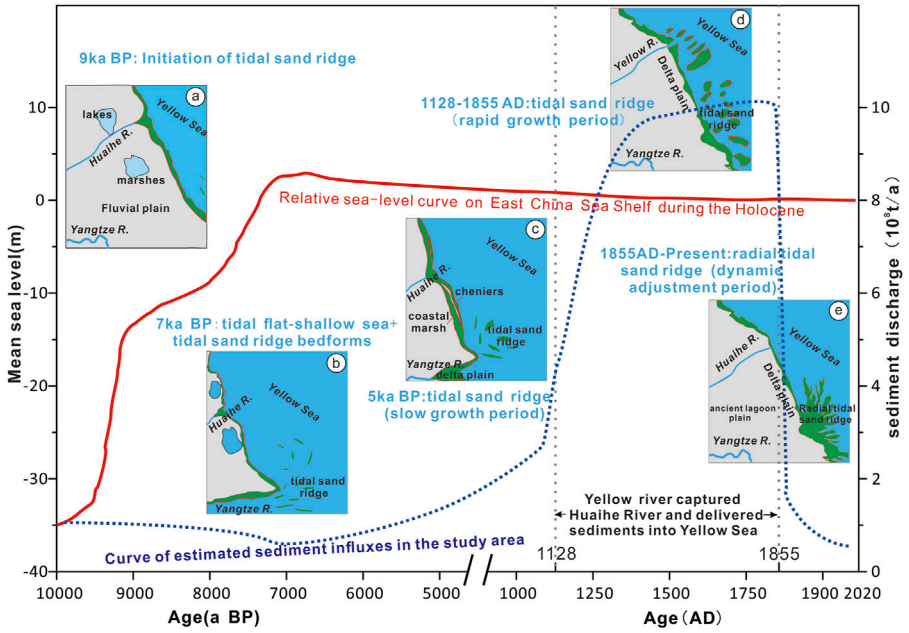

FIGURE 12
Synoptic geomorphological diagram revealing the relationships between Holocene evolution of the tidal sand ridge and relative sea-level change and sediment supply in the south Yellow Sea. The relative sea-level curve on the East China Sea shelf is modified from Xue (2014). The curve of estimated sediment influxes in the study area is referred to as the estimated sediment discharge of the Yellow River by Wang et al. (2007a). **(A)** 9 ka BP: initiation of tidal sand ridge bedforms during the rapid sea-level rise at the early Holocene; **(B)** 7 ka BP: the tidal flat and shallow sea environments well developed in the study area during the Holocene maximum transgressive period. The tidal sand ridge may mostly occur outside the Yangtze River mouth according to Li et al. (2001); **(C)** 5 ka BP: the tidal sand ridge developed slowly in the south Yellow Sea, while the cheniers and coastal marshes are well developed in the coastal area (Wang and Ke, 1989); **(D)** 1128–1855 AD: rapid growth of the tidal sand ridge after the Yellow River capturing the Huaihe River and subsequently delivering a large amount of sediment into the study area; and **(E)** 1855 AD–present: dynamic adjustment of the radial tidal sand ridge after the Yellow River emptying back into the Bohai Sea.

reconstructed from the core JSWZK01 (Figure 9), confirming that tidal sand deposition occurred during the Holocene transgression.

5.2.6 7,000–1,128 cal a BP

The Holocene maximum marine ingression took place around 7,000 cal a BP in the SYS region (Liu et al., 2004; Xue, 2014—Figures 8–10, 12B). Previous model simulations revealed that the apex of the radial tidal current was located at the paleo Yangtze River Channel mouth (Uehara et al., 2002; Figure 12B). In the southern region, tidal sand ridges gradually received more abundant supplies of sediment, while in the northern part, sedimentation occurred in a shallow marine environment and a chenier–coastal marsh sedimentary system on the landward side (Figure 12C; Wang and Ke, 1989). As the coastline prograded seaward after 7,000 cal a BP, the study area was gradually subdivided into a northern (deltaic) area and a southern (tidal sand ridge) area.

5.2.7 1128–1855 AD

The Yellow River captured the Huaihe River from the north of Jiangsu to the sea after 1128 AD (Liu et al., 2013). With 1 billion tons of sediment discharge into the south Yellow Sea per year, a new Yellow River Delta lobe formed in the north of Jiangsu, and the shoreline migrated southward at an average rate of 250–300 m/a (Zhang, 1984). Moreover, a large subaqueous delta also emerged in the northern part of the study area (Zhou et al., 2014; Figure 1B; Figures 8, 10). During this period, the tidal sand ridge system was fed by a huge amount of sediment, which is reflected in very high sediment accumulation rates (Figure 11), and the size of the RTSR dramatically increased in height and width (Liu and Xia, 2004). The submerged sand ridges gradually emerged, especially their nearshore portion (Figure 12D; see several ancient charts collected by Su et al., 2017a).

5.2.8 After 1855 AD

The Yellow River went back to the Bohai Sea after 1855 AD, and the Jiangsu Yellow River Delta was abandoned. The Jiangsu coastline and underwater bedforms were continuously and dynamically adjusted with the abrupt decrease in sediment influx (Zhou et al., 2014). The abandoned subaqueous delta suffered severe erosion under the combined effect of tidal currents and alongshore waves (Liu et al., 2013). Meanwhile, the huge deposit left by the Yellow River was gradually shaped by tidal currents into a new submarine linear bedform (Liu and Xia, 2004). This bedform combined with the southern sand ridges to form the present Jiangsu offshore sand ridge system (Figure 12E; Su et al., 2017b).

5.3 Controlling factors on the formation and evolution of the RTSR

Previous studies highlighted that sand ridge formation, growth, migration, and eventual drowning on storm-dominated shelves are the results of geologic processes (i.e., relative sea-level rise and shoreline transgression), oceanographic processes (i.e., storms and offshore-directed currents), and other factors (sediment supply and antecedent

geology) (Figueiredo et al., 1981; McBride and Moslow, 1991; Nnafie et al., 2014). These factors can also be essential to explain the distribution, evolution, and morphology of the RTSR on the tide-dominated Yellow Sea shelf.

5.3.1 Relative sea-level rise and marine transgression

Holocene coastal and shelf sedimentary systems, including the sand ridge facies, were sensitive to sea-level changes in the East China Sea (Gao and Collins, 2014; Li et al., 2014). The same holds for Late Pleistocene sea-level changes, which clearly affected the sedimentary evolution of the shelf in our study area.

The magnitude of eustatic rise since the Late Pleistocene primarily controlled the formation of sand ridge facies in the SYS. Previous research on paleo sea-level reconstructions indicated that the extent of the MIS 3 transgression was smaller than that of the Holocene and MIS 5 ages (Chappell et al., 1996). This implies that no sufficient accommodation was created in the Yellow Sea to host a thick tidal system during this period. Indeed, an alternation of terrestrial and marine facies prevailed in the northern region, and barely no marine facies developed in the south during MIS 3 (Figure 10). In contrast, at least 15-m-thick tidal sand ridge facies accumulated in the study boreholes during the Holocene and MIS 5 (See Figure 9, 10).

In addition, changes in the rates of relative sea-level rise likely affected sand ridge growth and migration in the SYS shelf. Liu et al. (2004) outlined a classical stepwise post-glacial sea-level rise in the western Pacific and postulated a close tie between phases of rapid relative sea-level rise and distinct meltwater pulse events. Rapid relative sea-level rise, especially in the early Holocene around 9,000 cal a BP, largely favored the development of transgressive depositional systems, including the sand ridge facies (Hori and Saito, 2007; Xia et al., 2012). Sand ridges developed as bedforms or sandy shoals during this phase of rapid relative sea-level rise and migrated landward under continuing transgression. When the relative sea-level rise decelerated and kept steady after 7,000 cal a BP, the tide-wave system had enough time to shape the sandy bedforms or shoals into the final form of the RTSR.

5.3.2 Sediment supply

Sediment provenance is another aspect of debate about the evolution of the RTSR. Based on the interpretation of shallow seismic profiles and stratigraphic correlation between the northern Jiangsu plain and Yangtze River Delta, early studies indicated that the tidal sand ridge area represented an independent "desert accumulation" during the LGM (Zhao, 1991). However, based on grain size analysis and the clastic mineral composition of sediments in the tidal sand ridge area, Wang et al. (1999) proposed that the sediments of the RTSR were mainly derived from the ancient Yangtze River. This hypothesis has been recently supported by detrital zircon geochronology in the SYS (Su et al., 2018). However, based upon heavy minerals and geochemical analysis from cores in the northern Jiangsu land area and in the tidal sand ridge area, most researchers believe that the ancient Yellow River and Yangtze River catchments were the major sediment sources for the RTSR, with the relative influence of each river depending on the distance from the ancient river mouth (Li et al., 2001; Yang et al., 2002; Wang Y. et al., 2009; Wang et al., 2013; Wang Z. B. et al., 2019). Moreover, Liu and Xia (2004) postulated multiple sources for the sand ridge systems: 1) Yellow River provenance for its southern part, mainly supplied in the historical period; 2) Yangtze River provenance for the southern sand ridge; and 3) glacial terrestrial sediments for the SYS shelf.

Although the debate is still open, most authors agree that a huge amount of sediment was necessary for the development of the enormous RTSR in the SYS (Li and Zhao, 1995; Zhu, 1998). Our age–depth plot of core data may provide new insights into this subject. The rates of tidal sand ridges were consistently 1.1–3.3 mm/a before 1128 AD, slightly 2–3 times than the average sedimentary rate on the SYS shelf, and dramatically increased to 18.9–108.7 mm/a after 1128 AD. We, thus, believe that the Yellow River played a key role in the rapid accretion (growth) of the RTSR through enormous sediment input into the Yellow Sea during 1128–1855 AD.

5.3.3 Oceanographic processes

The morphology of sand ridges on terrigenous shelves is generally parallel to the dominant current flow. This is particularly clear for the tidal sand ridges on the SYS shelf (Figure 1A). In this area, the radial morphology of the RTSR coincides with the directions of the current flow in the present radial tidal field (Wang, 2002).

There is some uncertainty about the relationship between ancient ocean dynamics and sand ridge growth in the study area. Although several hydrodynamic model simulations revealed that the radial tidal field could have formed off the Jiangsu Coast around 10,000–8,500 a BP, the radial center of tidal currents migrated north and south repeatedly, following the movement of the Jiangsu paleocoastline (Li et al., 2001; Uehara et al., 2002). This means that the formation and migration of the sand ridges could have been very complex due to unpredictable hydrodynamic conditions since the early Holocene in the SYS area.

As a matter of fact, the typical morphology of the RTSR became radial in shape only after 1900 AD, which is consistent with previous ancient charts (Zhang, 1988). In addition, wave currents appear to have dominated the Jiangsu Coast, leading to the formation of coastal barrier–lagoon systems in the northern Jiangsu coastal plain between ~8,500 a BP and 1128 AD (see studies of shelly sand bars by Wang and Ke, 1989; Ling, 2002; Xue et al., 2010). A large amount of Yellow River sediments emptied into the Yellow Sea and filled the Jiangsu Coast during 1128–1855 AD, resulting in the formation of the northern Jiangsu Yellow River Delta (Xue et al., 2010). In the meanwhile, the SYS shelf became wide and had a low gradient, which likely weakened wave activity and strengthened the influence of local tidal currents. After the Yellow River re-entered the Bohai Sea, tidal currents played a prominent role in redistributing the abandoned subaqueous deltaic sediments, shaping the irregular morphologies of the sand ridges into their present radial form (Liu and Xia, 2004).

6 Conclusion

A total of 10 ~30–60 m-long cores were retrieved from the Jiangsu coastal plain and offshore a sand ridge field in the south Yellow Sea (SYS) during 2018–2019. Based on a comprehensive analysis of sedimentary facies, grain size, foraminifers, radiocarbon dates (AMS ^{14}C), and optically stimulated luminescence (OSL) ages, we reconstructed the detailed Late Pleistocene sedimentary evolution of the radial tidal sand ridge (RTSR) region. This area evolved from a tidal sand ridge system during the late MIS 5 to an alluvial plain, with river channels and

floodplains during MIS 4. A deltaic sedimentary system, reconstructed in the northern part of the RTSR region, developed approximately in the early MIS 3. After a period of fluvial incision, channel belt sedimentation, and paleosol formation during the Last Glacial Maximum, the RTSR began to form during the early Holocene. Our stratigraphic correlation of along-dip and along-strike transects indicates that deltas and tidal sand ridges are important sedimentary components in this region, representing the relative sea-level change history since the Late Pleistocene. Age–depth plots reveal that the RTSR likely initiated in a sandy bedform shape at approximately 9,000 cal a BP, with sedimentation rates of 1.1–3.3 mm/a and continued throughout the Holocene. Sedimentation rates increased rapidly to 18.9–108.7 mm/a after 1128 AD, when the Yellow River captured the Huaihe River, flowing southward into the Yellow Sea. This study suggests that increased sediment supply played a major role in the formation and evolution of the Holocene RTSR in the south Yellow Sea. Relative sea-level change created sufficient accommodation to host a thick tidal system during this period in the SYS and also likely affected sand ridge growth and migration by changing the rates of relative sea-level rise in the SYS shelf. Oceanographic processes, namely, the radial current flow in the SYS, dominated the formation of radial morphology in the RTSR. Thus, our studies also highlight that relative sea-level change and oceanographic processes were important controlling factors of the distribution, evolution, and morphology of the RTSR on the tide-dominated Yellow Sea shelf.

Data availability statement

The original contributions presented in the study are included in the article/Supplementary Material; further inquiries can be directed to the corresponding author.

Author contributions

LH: writing and editing—original draft. SY: project administration. CX: conceptualization and methodology. GZ: investigation. SY: visualization. AA: writing—review and editing and supervision.

Funding

This research was jointly supported by Laoshan Laboratory (LSKJ202204003), China Geological Survey projects (Grant Nos. DD20189503, DD20221775), Asian Cooperation Fund (Comparative Study of geoenvironment and Geohazards in the Yangtze River Delta and the Red River Delta) and the National Natural Science Foundation of China (Grant Nos. U22A20558, 42076070).

Acknowledgments

The authors thank Hongming Yuan, Xigui Ding, Guohua Hou, Shaofeng Pei, Liujuan Xie, Dapeng Su, Liangyong Zhou, Xiaoyong Duan, and Jian Liu for their help in the geological survey or in manuscript preparation. They also thank Dr. Dario Gioia (editor), Dr. Domenico Chiarella, and another reviewer for their helpful comments on an earlier draft of this paper.

Conflict of interest

The authors declare that the research was conducted in the absence of any commercial or financial relationships that could be construed as a potential conflict of interest.

Publisher's note

All claims expressed in this article are solely those of the authors and do not necessarily represent those of their affiliated organizations, or those of the publisher, the editors, and the reviewers. Any product that may be evaluated in this article, or claim that may be made by its manufacturer, is not guaranteed or endorsed by the publisher.

Supplementary material

The Supplementary Material for this article can be found online at: https://www.frontiersin.org/articles/10.3389/feart.2022.1107495/full#supplementary-material

References

Abrahim, B. M. S., Nichol, S. L., Parker, R. J., and Gregory, M. R. (2008). Facies depositional setting, mineral maturity and sequence stratigraphy of a Holocene drowned valley, Tamaki Estuary, New Zealand. *Estuar. Coast. Shelf S.* 79, 133–142. doi:10.1016/j.ecss.2008.03.007

Amorosi, A., Pavesi, M., Lucchi, M. R., Sarti, G., and Piccin, A. (2008). Climatic signature of cyclic fluvial architecture from the Quaternary of the central Po Plain. *Italy. Sediment. Geol.* 209, 58–68. doi:10.1016/j.sedgeo.2008.06.010

Amorosi, A., Bruno, L., Cleveland, D. M., Morelli, A., and Hong, W. (2017). Paleosols and associated channel-belt sand bodies from a continuously subsiding late Quaternary system (Po Basin, Italy): New insights into continental sequence stratigraphy. *Geol. Soc. Am. Bull.* 129, 449–463. doi:10.1130/b31575.1

Amos, C., and King, E. (1984). Bedforms of the Canadian eastern seaboard: a comparison with global occurrences. *Mar. Geol.* 57, 167–208. doi:10.1016/0025-3227(84)90199-3

Antia, E. (1996). Shoreface-connected ridges in German and US mid-atlantic bights: similarities and contrasts. *J. Coast. Res.* 12, 141–146.

Beardsley, R. (1983). "Structure of the changjiang river plume in the East China Sea during june 1980," in Proceedings of International Symposium on Sedimentation on the Continental Shelf, with Special Reference to the East China Sea (China Ocean Press), 265–284.

Berne, S., Lericolais, G., Marsset, T., Bourillet, J. F., and De Batist, M. (1998). Erosional offshore sand ridges and lowstand shorefaces; examples from tide-and wave-dominated environments of France. *J. Sediment. Res.* 68, 540–555. doi:10.2110/jsr.68.540

Berne, S., Vagner, P., Guichard, F., Lericolais, G., Liu, Z., Trentesaux, A., et al. (2002). Pleistocene forced regressions and tidal sand ridges in the East China Sea. *Mar. Geol.* 188, 293–315. doi:10.1016/s0025-3227(02)00446-2

Brenner, R. L. (1980). Construction of process-response models for ancient epicontinental seaway depositional systems using partial analogs. *AAPG Bull.* 64, 1223–1244.

Calvete, D., Walgreen, M., De Swart, H., and Falqués, A. (2001). A model for sand ridges on the shelf: Effect of tidal and steady currents. *J. Geophys. Res-Oceans* 106, 9311–9325. doi:10.1029/2001jc900001

Chappell, J., Omura, A., Esat, T., McCulloch, M., Pandolfi, J., Ota, Y., et al. (1996). Reconciliaion of late Quaternary sea levels derived from coral terraces at Huon Peninsula with deep sea oxygen isotope records. *Earth Planet. Sci. Lett.* 141, 227–236. doi:10.1016/0012-821x(96)00062-3

Chen, B., Li, C., and Ye, Z. (1995). A study on the Holocene buried tidal sand bodies in the south Yellow Sea coastal land (in Chinese with English abstract). *Acta Geol. Sin.* 50, 447–458.

Cheng, G., and Xue, C. (1997). *Sedimentary geology of Yellow River Delta*. Beijing: Geological publishing House, 1–47. (in Chinese).

Chiarella, D., Longhitano, S. G., Mosdell, W., and Telesca, D. (2020). Sedimentology and facies analysis of ancient sand ridges: Jurassic Rogn Formation, Trøndelag Platform, offshore Norway. *Mar. Pet. Geol.* 112, 104082. doi:10.1016/j.marpetgeo.2019.104082

Chough, S. K., Lee, H. J., Chun, S. S., and Shinn, Y. J. (2004). Depositional processes of late quaternary sediments in the Yellow Sea: a review. *Geosci. J.* 8, 211–264. doi:10.1007/bf02910197

Coleman, J. M., and Wright, L. D. (1975). *Modern River deltas: Variability of processes and sand bodies*. Houston: Houston Geological Society.

Como, S., and Magni, P. (2009). Temporal changes of a macrobenthic assemblage in harsh lagoon sediments. *Estuar. Coast. Shelf S.* 83, 638–646. doi:10.1016/j.ecss.2009.05.024

Davis, R. A., and Balson, P. S. (1992). Stratigraphy of a North Sea tidal sand ridge. *J. Sediment. Res.* 62, 116–121.

Davis, R. A., Klay, J., and Jewell, P. (1993). Sedimentology and stratigraphy of tidal sand ridges southwest Florida inner shelf. *J. Sediment. Res.* 63, 91–104.

Emery, K. (1968). Relict sediments on continental shelves of world. *AAPG Bull.* 52, 445–464.

Figueiredo, A. G., Swift, D. J. P., and Clarke, T. L. (1981). Sand ridges on the inner Atlantic shelf of North America: Morphometric comparisons with Huthnance stability model. *Geo.-Mar. Lett.* 1 (3), 187–191. doi:10.1007/BF02462432

Figueiredo, A. G., Sanders, J. E., and Swift, D. J. (1982). Storm-graded layers on inner continental shelves: Examples from southern Brazil and the Atlantic coast of the central United States. *Sediment. Geol.* 31, 171–190. doi:10.1016/0037-0738(82)90057-4

Folk, R. L., and Ward, W. C. (1957). Brazos River bar: a study in the significance of grain size parameters. *J. Sediment. Petrol.* 31, 514–519.

Galloway, W. E., and Hobday, D. K. (1983). *Terrigenous clastic depositional systems: applications to petroleum, coal, and uranium exploration*. New York: Springer.

Gao, S., and Collins, M. (2014). Holocene sedimentary systems on continental shelves. *Mar. Geol.* 352, 268–294. doi:10.1016/j.margeo.2014.03.021

Gao, L., Long, H., Tamura, T., Hou, Y., and Shen, J. (2021). A ~130 ka terrestrial-marine interaction sedimentary history of the northern Jiangsu coastal plain in China. *Mar. Geol.* 435, 106455. doi:10.1016/j.margeo.2021.106455

Gao, S. (2009). Modeling the preservation potential of tidal flat sedimentary records, Jiangsu coast, eastern China. *Cont. Shelf Res.* 29, 1927–1936. doi:10.1016/j.csr.2008.12.010

Geng, X., Wan, Y., Li, S., Zhang, Q., and Xu, X. (1983). Evolutionary process of Northern Jiangsu coastal zone and a dynamic equilibrium model of Northern Jiangsu shoal (in Chinese with English abstract). *Acta Oceanol. Sin.* 2, 284–298.

Goff, J. A., Swift, D. J., Duncan, C. S., Mayer, L. A., and Hughes-Clarke, J. (1999). High-resolution swath sonar investigation of sand ridge, dune and ribbon morphology in the offshore environment of the New Jersey margin. *Mar. Geol.* 161, 307–337. doi:10.1016/s0025-3227(99)00073-0

Green, M. O. (1986). Side-scan sonar mosaic of a sand ridge field: Southern Mid-Atlantic Bight. *Geo-mar. Lett.* 6, 35–40. doi:10.1007/bf02311694

He, L., Xue, C., Ye, S., Laws, E. A., Yuan, H., Yang, S., et al. (2018). Holocene evolution of the Liaohe Delta, a tide-dominated delta formed by multiple rivers in Northeast China. *J. Asian Earth Sci.* 152, 52–68. doi:10.1016/j.jseaes.2017.11.035

He, L., Xue, C., Ye, S., Amorosi, A., Yuan, H., Yang, S., et al. (2019). New evidence on the spatial-temporal distribution of superlobes in the Yellow River Delta complex. *Quat. Sci. Rev.* 214, 117–138. doi:10.1016/j.quascirev.2019.05.003

Hoogendoorn, E. L., and Dalrymple, R. W. (1986). Morphology, lateral migration, and internal structures of shoreface-connected ridges, Sable Island Bank, Nova Scotia, Canada. *Geology* 14, 400–403. doi:10.1130/0091-7613(1986)14<400:mlmais>2.0.co;2

Hori, K., and Saito, Y. (2007). An early Holocene sea-level jump and delta initiation. *Geophy. Res. Lett.* 34, L18401. doi:10.1029/2007gl031029

Hori, K., Saito, Y., Zhao, Q., Cheng, X., Wang, P., Sato, Y., et al. (2001). Sedimentary facies of the tide-dominated paleo-Changjiang (Yangtze) estuary during the last transgression. *Mar. Geol.* 177, 331–351. doi:10.1016/s0025-3227(01)00165-7

Hori, K., Tanabe, S., Saito, Y., Haruyama, S., Nguyen, V., and Kitamura, A. (2004). Delta initiation and Holocene seasea-level change: example from the Song hong (Red River) delta, vietnam. *Vietnam. Sediment. Geol.* 164, 237–249. doi:10.1016/j.sedgeo.2003.10.008

Houbolt, J. J. H. C. (1968). Recent sediments in the southern bight of the North Sea. *Geol. Mijnb.* 47, 245–273.

Ji, Y., Yin, Y., Li, Q., and Wang, A. (2015). The core-recorded strata and environmental changes since the Late Pleistocene in Kushuiyang area of the radial tidal sandy ridge system, Jiangsu offshore, southern Yellow Sea. *J. Nanjing Univ. (Nat. Sci.)* 51 (3), 641–657. doi:10.13232/j.cnki.jnju.2015.03.020

Johnson, H. D. (1977). Shallow marine sand bar sequences: an example from the late precambrian of North Norway. *Sedimentology* 24, 245–270. doi:10.1111/j.1365-3091.1977.tb00256.x

Jung, W., Suk, B., Min, G., and Lee, a. K. (1998). Sedimentary structure and origin of a mud-cored pseudo-tidal sand ridge, eastern Yellow Sea, Korea. *Mar. Geol.* 151, 73–88. doi:10.1016/s0025-3227(98)00058-9

Knobles, D., Wilson, P., Goff, J., and Cho, S. (2008). Seabed acoustics of a sand ridge on the New Jersey continental shelf. *J. Acoust. Soc. Am.* 124, 151–156. doi:10.1121/1.2960977

Krumbein, W. C., and Sloss, L. L. (1963). *Stratigraphy and sedimentation*. San Francisco: Free Man.

Lan, S., Gu, C., and Fu, B. (1986). Characteristics of temperature and salinity of the southern Yellow sea warm current water (in Chinese with English abstract). *Stud. Mar. Sin.* 27, 45–53.

Lee, J. H., Pang, I. C., Moon, I. J., and Ryu, J. H. (2011). On physical factors that controlled the massive green tide occurrence along the southern coast of the Shandong Peninsula in 2008: A numerical study using a particle-tracking experiment. *J. Geophys. Res-Oceans* 116, C12036. doi:10.1029/2011jc007512

Lei, Y., He, L., Ye, S., Zhao, L., Yuan, H., Yang, S., et al. (2021). Paleochannel distribution, delta development and paleoenvironment evolution in Bohai Bay since the Late Pleistocene. *Geol. China* 48 (6), 1947–1964. (in Chinese with English abstract). doi:10.12029/gc20210621

Li, C., and Wang, P. (1991). Stratigraphy of the Late Quaternary barrier-lagoon depositional systems along the coast of China. *Sediment. Geol.* 72, 189–200. doi:10.1016/0037-0738(91)90011-2

Li, Q., and Yin, Y. (2013). Sedimentary facies and evolution of the Likejiao sandy ridge, in the South Yellow Sea offshore area, eastern China. *Geogr. Res.* 32, 1843–1855. in Chinese with English abstract. doi:10.11821/dlyj201310008

Li, C., and Zhao, J. (1995). Recent research and controversy of the Jianggang radial sand ridge in Northern Jiangsu Province (in Chinese). *Mar. Sci.* 4, 58–60. doi:10.11759/HYKX.0.1995-04-016

Li, C., Zhang, J., and Deng, B. (2001). Holocene regression and the tidal radial sand ridge system formation in the Jiangsu coastal zone, east China. *Mar. Geol.* 173, 97–120. doi:10.1016/s0025-3227(00)00169-9

Li, C., Wang, P., Sun, H., Zhang, J., Fan, D., and Deng, B. (2002). Late quaternary incised-valley fill of the Yangtze delta (China): its stratigraphic framework and evolution. *Sediment. Geol.* 152, 133–158. doi:10.1016/s0037-0738(02)00066-0

Li, G., Li, P., Liu, Y., Qiao, L., Ma, Y., Xu, J., et al. (2014). Sedimentary system response to the global sea level change in the East China Seas since the last glacial maximum. *Earth Sci. Rev.* 139, 390–405. doi:10.1016/j.earscirev.2014.09.007

Liao, H., and Yu, H. (2005). Morphology, hydrodynamics and sediment characteristics of the Changyun sand ridge offshore Western Taiwan. *Terr. Atmos. Ocean. Sci.* 16, 621–640. doi:10.3319/tao.2005.16.3.621(t)

Ling, S. (2002). Study on the dynamic changes of coastline in north Jiangsu since the Holocene. *J. Oceanogr. Huanghai Bohai Seas.* 20, 37–46. in Chinese with English abstract.

Liu, Z., and Xia, D. (2004). *Tidal sands in the China seas*. Beijing: China Ocean Press. in Chinese with English abstract.

Liu, Z., Huang, Y., and Zhang, Q. (1989). Tidal current ridges in the southwestern Yellow Sea. *J. Sediment. Res.* 59, 432–437. doi:10.1111/j.1538-7836.2004.00794.x

Liu, Z., Xia, D., Berne, S., Wang, K., Tang, M., Tang, Y., et al. (1998). Tidal deposition systems of China's continental shelf, with special reference to the eastern Bohai Sea. *Mar. Geol.* 145, 225–253. doi:10.1016/s0025-3227(97)00116-3

Liu, J. P., Milliman, J. D., Gao, S., and Cheng, P. (2004). Holocene development of the Yellow River's subaqueous delta, North Yellow sea. *Mar. Geol.* 209, 45–67. doi:10.1016/j.margeo.2004.06.009

Liu, Z., Berné, S., Saito, Y., Yu, H., Trentesaux, A., Uehara, K., et al. (2007). Internal architecture and mobility of tidal sand ridges in the East China Sea. *Cont. Shelf Res.* 27, 1820–1834. doi:10.1016/j.csr.2007.03.002

Liu, J., Saito, Y., Wang, H., Zhou, L., and Yang, Z. (2009). Stratigraphic development during the late pleistocene and Holocene offshore of the Yellow River delta, Bohai Sea. *J. Asian Earth Sci.* 36, 318–331. doi:10.1016/j.jseaes.2009.06.007

Liu, J., Saito, Y., Kong, X., Wang, H., Wen, C., Yang, Z., et al. (2010). Delta development and channel incision during marine isotope stages 3 and 2 in the Western South Yellow Sea. *Mar. Geol.* 278, 54–76. doi:10.1016/j.margeo.2010.09.003

Liu, J., Kong, X., Saito, Y., Liu, J. P., Yang, Z., and Wen, C. (2013). Subaqueous deltaic formation of the old Yellow River (AD 1128-1855) on the Western South Yellow sea. *Mar. Geol.* 344, 19–33. doi:10.1016/j.margeo.2013.07.003

Liu, J., Wang, H., Wang, F., Qiu, J., Saito, Y., Lu, J., et al. (2016). Sedimentary evolution during the last ~1.9 Ma near the Western margin of the modern Bohai Sea. *Palaeogeogr. Palaeocl.* 451, 84–96. doi:10.1016/j.palaeo.2016.03.012

Liu, B., Wu, H., Zhang, Z., Wei, G., Wang, Y., Zheng, J., et al. (2021). Recent evolution of the intertidal sand ridge lines of the dongsha shoal in the modern radial Sand Ridges, east China. *Int. J. Env. Res. Pub. He.* 18, 1573. doi:10.3390/ijerph18041573

Longhitano, S. G., Rossi, V. M., Chiarella, D., Mellere, D., Tropeano, M., Dalrymple, R. W., et al. (2021). Anatomy of a mixed bioclastic–siliciclastic regressive tidal sand ridge: Facies-based case study from the lower Pleistocene Siderno Strait, southern Italy. *Sedimentology* 68 (6), 2293–2333. doi:10.1111/sed.12853

McBride, R. A., and Moslow, T. F. (1991). Origin, evolution, and distribution of shoreface sand ridges, Atlantic inner shelf, USA. *Mar. Geol.* 97, 57–85. doi:10.1016/0025-3227(91)90019-z

McClennan, C., and McMaster, R. (1971). Probable Holocene transgressive effects on the geomorphic features of the continental shelf off New Jersey, United States. *Atl. Geol.* 7, 69–72. doi:10.4138/1944

Miall, A. D. (1992). "Alluvial deposits," in *Facies models: Response to sea level change*. Editors R. G. Walker and N. P. James (Waterloo: Geological Association of Canada), 119–139.

Murray, A. S., and Wintle, A. G. (2000). Luminescence dating of quartz using an improved single-aliquot regenerative-dose protocol. *Radiat. Meas.* 32, 57–73. doi:10.1016/s1350-4487(99)00253-x

Mycielska-Dowgiałło, E., and Ludwikowska-Kędzia, M. (2011). Alternative interpretations of grain-size data from Quaternary deposits. *Geologos* 17, 189–203. doi:10.2478/v10118-011-0010-9

Nnafie, A., De Swart, H., Calvete, D., and Garnier, R. (2014). Effects of sea level rise on the formation and drowning of shoreface-connected sand ridges, a model study. *Cont. Shelf Res.* 80, 32–48. doi:10.1016/j.csr.2014.02.017

Park, S., and Lee, S. (1994). Depositional patterns of sand ridges in tide-dominated shallow water environments: Yellow Sea coast and South Sea of Korea. *Mar. Geol.* 120, 89–103. doi:10.1016/0025-3227(94)90079-5

Park, S., Han, H., and Yoo, D. (2003). Transgressive sand ridges on the mid-shelf of the southern sea of Korea (Korea strait): formation and development in high-energy environments. *Mar. Geol.* 193, 1–18. doi:10.1016/s0025-3227(02)00611-4

Park, S., Lee, B., Han, H., Yoo, D., and Lee, C. (2006). Late Quaternary stratigraphy and development of tidal sand ridges in the eastern Yellow Sea. *J. Sediment. Res.* 76, 1093–1105. doi:10.2110/jsr.2006.092

Parker, G., Lanfredi, N. W., and Swift, D. J. (1982). Seafloor response to flow in a southern hemisphere sand-ridge field: Argentine inner shelf. *Sediment. Geol.* 33, 195–216. doi:10.1016/0037-0738(82)90055-0

Pendleton, E. A., Brothers, L. L., Thieler, E. R., and Sweeney, E. M. (2017). Sand ridge morphology and bedform migration patterns derived from bathymetry and backscatter on the inner-continental shelf offshore of Assateague Island, USA. *Cont. Shelf Res.* 144, 80–97. doi:10.1016/j.csr.2017.06.021

Rao, W., Mao, C., Wang, Y., Su, J., Balsam, W., and Ji, J. (2015). Geochemical constraints on the provenance of surface sediments of radial sand ridges off the Jiangsu coastal zone, East China. *Mar. Geol.* 359, 35–49. doi:10.1016/j.margeo.2014.11.007

Reimer, P. J., Bard, E., Bayliss, A., Beck, J. W., Blackwell, P. G., Ramsey, C. B., et al. (2013). Intcal 13 and Marine13 radiocarbon age calibration curves 0-50, 000 years cal BP. *Radiocarbon* 55, 1869–1887. doi:10.2458/azu_js_rc.55.16947

Ren, M., and Shi, Y. (1986). Sediment discharge of the Yellow River (China) and its effect on the sedimentation of the Bohai and the Yellow Sea. *Cont. Shelf Res.* 6 (6), 785–810. doi:10.1016/0278-4343(86)90037-3

Ren, M. (1986). *Comprehensive investigation of coastal zone and tidal flat Resources*. Beijing: China Ocean Press. Jiangsu Province.

Reynaud, J. Y., Tessier, B., Proust, J. N., Dalrymple, R., Marsset, T., De Batist, M., et al. (1999). Eustatic and hydrodynamic controls on the architecture of a deep shelf sand bank (Celtic Sea). *Sedimentology* 46, 703–721. doi:10.1046/j.1365-3091.1999.00244.x

Ridente, D. (2018). Late pleistocene post-glacial sea level rise and differential preservation of transgressive "sand ridge" deposits in the Adriatic sea. *Geosciences* 8, 61. doi:10.3390/geosciences8020061

Saito, Y., Yang, Z., and Hori, K. (2001). The huanghe (Yellow River) and changjiang (Yangtze River) deltas: a review on their characteristics, evolution and sediment discharge during the Holocene. *Geomorphology* 41, 219–231. doi:10.1016/s0169-555x(01)00118-0

Saito, Y. (1989). Late Pleistocene coastal sediments, drainage patterns and sand ridge systems on the shelf off Sendai, northeast Japan. *Mar. Geol.* 89, 229–244. doi:10.1016/0025-3227(89)90077-7

Shi, W., Wang, M., Li, X., and Pichel, W. G. (2011). Ocean sand ridge signatures in the Bohai Sea observed by satellite ocean color and synthetic aperture radar measurements. *Remote Sens. Environ.* 115, 1926–1934. doi:10.1016/j.rse.2011.03.015

Snedden, J. W., and Dalrymple, R. W. (1999). "Modern shelf sand ridges: from historical perspective to a unified hydrodynamic and evolutionary model," in *Isolated shallow marine sand bodies: Sequence stratigraphic analysis and sedimentologic interpretation*. Editors K. M. Bergman and J. W. Snedden (SEPM), 13–28.

Snedden, J. W., Tillman, R. W., and Culver, S. J. (2011). Genesis and evolution of a mid-shelf, storm-built sand ridge, New Jersey continental shelf, USA. *J. Sediment. Res.* 81, 534–552. doi:10.2110/jsr.2011.26

Song, D., Gao, Z., Xu, F., Ai, J., Ning, J., Shang, W., et al. (2018). Spatial and temporal variability of the green tide in the South Yellow Sea in 2017 deciphered from the GOCI image. *Oceanol. Limnol. Sinic* 49 (5), 1068–1074. in Chinese with English abstract.

Southon, J., Kashgarian, M., Fontugne, M., Metivier, B., and Yim, W. W. (2002). Marine reservoir corrections for the Indian ocean and southeast asia. *Radiocarbon* 44, 167–180. doi:10.1017/s0033822200064778

Stanley, D. J., and Chen, Z. (2000). Radiocarbon dates in China's Holocene Yangtze delta: record of sediment storage and reworking, not timing of deposition. *J. Coast. Res.* 16 (4), 1126–1132. doi:10.2307/4300129

Stride, A. H. (1982). "Ancient offshore tidal deposits," in *Offshore tidal sands: Processes and deposits*. Editor A. H. Stride (Dordrecht: Springer), 172–192.

Su, J., and Yuan, L. (2005). *China offshore hydrology*. Beijing: China Ocean Press. in Chinese.

Su, M., Yao, P., Wang, Z. B., Zhang, C. K., and Stive, M. J. (2017a). Exploratory morphodynamic hindcast of the evolution of the abandoned Yellow River delta, 1578–1855 CE. *Mar. Geol.* 383, 99–119. doi:10.1016/j.margeo.2016.11.007

Su, M., Yao, P., Wang, Z. B., Zhang, C. K., and Stive, M. J. (2017b). Exploratory morphodynamic modeling of the evolution of the Jiangsu coast, China, since 1855: Contributions of old Yellow River-derived sediment. *Mar. Geol.* 390, 306–320. doi:10.1016/j.margeo.2016.10.013

Su, J., Rao, W., Wang, Y., and Mao, C. (2018). Detrital zircon geochronology of the radial sand ridge system of jiangsu coast, east China: implication for sediment provenance. *J. Earth Sci.* 29, 144–154. doi:10.1007/s12583-017-0769-x

Sun, Z., Fang, W., Yong, Y., Gang, L., Song, G., and Xu, Q. (2014). Sedimentary environment evolution of Lanshayang tidal channel within the radial sand ridges, southern Yellow Sea. *J. Nanjing Univ. (Nat. Sci.)* 50, 553–563. in Chinese with English abstract. doi:10.13232/j.cnki.jnju.2014.05.003

Sun, Z., Li, G., and Yin, Y. (2015). The Yangtze River deposition in southern Yellow Sea during marine oxygen isotope stage 3 and its implications for sea-level changes. *Quat. Res.* 83, 204–215. doi:10.1016/j.yqres.2014.08.008

Swift, D. J., and Field, M. E. (1981). Evolution of a classic sand ridge field: Maryland sector, North American inner shelf. *Sedimentology* 28, 461–482. doi:10.1111/j.1365-3091.1981.tb01695.x

Swift, D. J., and Freeland, G. L. (1978). Current lineations and sand waves on the inner shelf, Middle Atlantic Bight of North America. *J. Sediment. Res.* 48, 1257–1266.

Swift, D. J., Holliday, B., Avignone, N., and Shideler, G. (1972). Anatomy of a shore face ridge system, False Cape, Virginia. *Mar. Geol.* 12, 59–84. doi:10.1016/0025-3227(72)90029-1

Swift, D. J., Parker, G., Lanfredi, N. W., Perillo, G., and Figge, K. (1978). Shoreface-connected sand ridges on American and European shelves: a comparison. *Estuar. Coast. Mar. Sci.* 7, 257–273. doi:10.1016/0302-3524(78)90109-3

Swift, D. J. (1975). Tidal sand ridges and shoal-retreat massifs. *Mar. Geol.* 18, 105–133. doi:10.1016/0025-3227(75)90007-9

Tanabe, S., Saito, Y., Vu, Q. L., Hanebuth, T. J. J., Ngo, Q. L., and Kitamura, A. (2006). Holocene evolution of the Song hong (Red River) delta system, northern vietnam. *Sediment. Geol.* 187, 29–61. doi:10.1016/j.sedgeo.2005.12.004

Trentesaux, A., Stolk, A., and Berne, S. (1999). Sedimentology and stratigraphy of a tidal sand bank in the southern North Sea. *Mar. Geol.* 159, 253–272. doi:10.1016/s0025-3227(99)00007-9

Trowbridge, J. (1995). A mechanism for the formation and maintenance of shore-oblique sand ridges on storm-dominated shelves. *J. Geophys. Res-Oceans* 100, 16071–16086. doi:10.1029/95jc01589

Twichell, D., Brooks, G., Gelfenbaum, G., Paskevich, V., and Donahue, B. (2003). Sand ridges off sarasota, Florida: A complex facies boundary on a low-energy inner shelf environment. *Mar. Geol.* 200, 243–262. doi:10.1016/s0025-3227(03)00185-3

Uehara, K., Saito, Y., and Hori, K. (2002). Paleotidal regime in the changjiang (Yangtze) estuary, the East China sea, and the Yellow Sea at 6 ka and 10 ka estimated from a numerical model. *Mar. Geol.* 183, 179–192. doi:10.1016/s0025-3227(01)00255-9

van de Meene, J. W., and van Rijn, L. C. (2000). The shoreface-connected ridges along the central Dutch coast—part 1: field observations. *Cont. Shelf Res.* 20, 2295–2323. doi:10.1016/S0278-4343(00)00048-0

Vis-Star, N. C., De Swart, H., and Calvete, D. (2007). Effect of wave-topography interactions on the formation of sand ridges on the shelf. *J. Geophys. Res-Oceans* 112, C06012. doi:10.1029/2006JC003844

Wagle, B., and Veerayya, M. (1996). Submerged sand ridges on the Western continental shelf off Bombay, India: evidence for late pleistocene-holocene sea-level changes. *Mar. Geol.* 136, 79–95. doi:10.1016/s0025-3227(96)00053-9

Wang, Y., and Ke, X. (1989). Cheniers on the east coastal plain of China. *Mar. Geol.* 90, 321–335. doi:10.1016/0025-3227(89)90134-5

Wang, X., and Ke, X. (1997). Grain-size characteristics of the extant tidal flat sediments along the Jiangsu coast, China. *Sediment. Geol.* 112, 105–122. doi:10.1016/s0037-0738(97)00026-2

Wang, Y., and Su, Y. (2013). Influence of solar activity on breaching, overflowing and course-shifting events of the Lower Yellow River in the late Holocene. *Holocene* 23 (5), 656–666. doi:10.1177/0959683612467481

Wang, P., Min, Q. B., and Bian, Y. H. (1985). "Distributions of foraminifera and ostracoda in bottom sediments of the northwestern part of the South Huanghai (Yellow) Sea and its geological significance," in *Marine micropaleontology of China*. Editor P. Wang (Beijing: China Ocean Press), 93–114. in Chinese.

Wang, J., Lu, G., Lin, H., Song, Z., and Jia, J. (1998). Developing process and mechanism of tidal sand ridges off the coast of jiangsu province. *J. Nanjing Norm. Univ. (Nat. Sci. ed.)* 21, 95–108. in Chinese with English abstract. doi:10.13232/j.NJSF.0.1998-03-022

Wang, Y., Zhu, D., You, K., Pan, S., Zhu, X., Zou, X., et al. (1999). Evolution of radiative sand ridge field of the South Yellow Sea and its sedimentary characteristics. *Sci. China Ser. D.* 42, 97–112. doi:10.1007/bf02878503

Wang, Y. H., Zhang, R. S., Xie, Z. R., and Wang, J. (2004). Relative Sea level changes and variational trends of the jiangsu radial sandbanks. *Adv. Mar. Sci.* 2, 198–203. in Chinese with English abstract. doi:10.3969/j.issn.1671-6647.2004.02.011

Wang, H., Yang, Z., Saito, Y., Liu, J. P., Sun, X., and Wang, Y. (2007a). Stepwise decreases of the Huanghe (Yellow River) sediment load (1950-2005): Impacts of climate change and human activities. *Glob. Planet. Change* 57, 331–354. doi:10.1016/j.gloplacha.2007.01.003

Wang, H., Zhang, X., Lan, X., Zhang, Z., Lin, Z., and Zhao, G. (2007b). Geochemistry characteristics of sediment and provenance relations of sediments in core NT1 of the south Yellow sea. *J. China Univ. Geosci.* 18, 287–298. doi:10.1016/s1002-0705(08)60009-6

Wang, S. J., Wang, L. M., Wan, Y. S., Zhang, C. J., and Wang, J. G. (2009). Study on intrusive rocks forming period and stages division in ludong area (in Chinese with English abstract). *Shandong Land Resour.* 25, 8–21.

Wang, Y., Wang, X., Gao, Y., Lv, H., and Zhang, X. (2009). A review on the reference material series for China Sea and continental shelf sediments. *Geol. China* 36, 1145–1153. in Chinese with English abstract.

Wang, Y., Zhang, Y., Zou, X., Zhu, D., and Piper, D. (2012). The sand ridge field of the South Yellow sea: Origin by river-sea interaction. *Mar. Geol.* 291, 132–146. doi:10.1016/j.margeo.2011.01.001

Wang, Y. Z., Gu, D. Q., Wang, W. H., and Qiao, L. L. (2012). The surface sediments size fraction and the distribution on lagoon and sand barriers in tangshan Bay. *Period. Ocean. Univ. China* 42, 131–136. in Chinese with English abstract. doi:10.16441/j.cnki.hdxb.2012.s1.019

Wang, K., Jiang, X., Ye, Q., Shi, X., and Liu, Y. (2013). Distribution and source of heavy minerals in the surface sediment of the tidal sand ridges area in south Yellow Sea (in Chinese with English abstract). *Mar. Geol. Quat. Geol.* 33, 1–11. doi:10.3724/sp.j.1140.2013.05001

Wang, L., Hu, S., Yu, G., Ma, M., and Liao, M. (2015). Paleoenvironmental reconstruction of the radial sand ridge field in the South Yellow Sea (east China) since 45 ka using the sediment magnetic properties and granulometry. *J. Appl. Geophys.* 122, 1–10. doi:10.1016/j.jappgeo.2015.08.002

Wang, L., Hu, S., Yu, G., Wang, X., Ma, M., Liao, M., et al. (2019a). Evolution of the radial sand ridge field in the southwestern Yellow Sea, China since the late MIS 3. *Z. für Geomorphol.* 62 (3), 217–229. doi:10.1127/zfg/2019/0640

Wang, L., Li, G., Xu, J., Liu, Y., Qiao, L., Ding, D., et al. (2019b). Strata sequence and paleochannel response to tectonic, sea-level, and Asian monsoon variability since the late Pleistocene in the South Yellow Sea. *Quat. Res.* 92, 450–468. doi:10.1017/qua.2019.29

Wang, Z. B., Li, R. H., Yang, S. Y., Bai, F. L., and Lu, K. (2019). Comparison of detrital mineral compositions between stream sediments of the Yangtze River (Changjiang) and the Yellow River (Huanghe) and their provenance implication. *China Geol.* 2, 169–178. doi:10.31035/cg2018065

Wang, Y. (2002). *Radiative sandy ridge field on continental shelf of the Yellow Sea*. Beijing: China Environmental Science Press. in Chinese.

Wu, Z., Jin, X., Zhou, J., Zhao, D., Shang, J., Li, S., et al. (2017). Comparison of buried sand ridges and regressive sand ridges on the outer shelf of the East China Sea. *Mar. Geophys. Res.* 38, 187–198. doi:10.1007/s11001-016-9278-z

Xia, F., and Zhang, Y. (2018). Late Quaternary strata and environmental evolution record of core LG in Longgang, north Jiangsu plain, China. *Geogr. Res.* 37, 433–446. in Chinese with English abstract. doi:10.11821/dlyj201802015

Xia, F., Yin, Y., Wang, Q., Zhang, Y., and Liu, J. P. (2012). Sequence stratigraphy of the central part of North Jiangsu coasts since late MIS 3, eastern China. *Acta Geol. Sin.* 86, 1696–1712. in Chinese with English abstract. doi:10.3969/j.issn.0001-5717.2012.10.009

Xia, F., Zhang, Y., Wang, Q., Yin, Y., Wegmann, K. W., and Liu, J. P. (2013). Evolution of sedimentary environments of the middle Jiangsu coast, South Yellow Sea since late MIS 3. *J. Geogr. Sci.* 23 (5), 883–914. doi:10.1007/s11442-013-1051-5

Xiao, N. (2015). "The sedimentary evolution research of coastal areas in Jianggang of Jiangsu province since Last Glacial Epoch," in *School of marine geosciences* (Qingdao: Ocean University of China), 75. in Chinese with English abstract.

Xu, M., Meng, K., Zhao, Y., and Zhao, L. (2019). Sedimentary environment evolution in east China's coastal tidal flats: The North Jiangsu radial sand ridges. *J. Coast. Res.* 35, 524–533. doi:10.2112/jcoastres-d-18-00006.1

Xue, C. (1993). Historical changes in the Yellow River delta, China. *Mar. Geol.* 113 (3–4), 321–330. doi:10.1016/0025-3227(93)90025-Q

Xue, C., Zhou, Y., and Wang, G. (2003). Reviews of the Yellow River Delta superlobes since 700 BC. *Mar. Geol. Quat. Geol.* 23, 23–29. in Chinese with English abstract. doi:10.16562/j.cnki.0256-1492.2003.03.005

Xue, C., Liu, J., and Kong, X. H. (2010). Preliminary study of Holocene Huaihe River Delta on west coastal plain of Yellow Sea, China. *Quat. Sci.* 30, 892–901. in Chinese with English abstract. doi:10.3969/j.issn.1001-7410.2010.05.06

Xue, C., Liu, J., and Kong, X. (2011). Channel shifting of lower Yellow River in 1128-1855AD and its influence to the sedimentation in Bohai, yellow and East China seas (in Chinese with English abstract). *Mar. Geol. Quat. Geol.* 31 (5), 25–36. doi:10.3724/sp.j.1140.2011.05025

Xue, C., Qin, Y., Ye, S., Laws, E. A., and Wang, Z. (2018). Evolution of Holocene ebb-tidal clinoform off the Shandong Peninsula on East China Sea shelf. *Earth-Sci. Rev.* 177, 478–496. doi:10.1016/j.earscirev.2017.12.012

Xue, C. (2014). Missing evidence for stepwise postglacial sea level rise and an approach to more precise determination of former sea levels on East China Sea Shelf. *Mar. Geol.* 348, 52–62. doi:10.1016/j.margeo.2013.12.004

Yang, S., Li, C., Jung, H., and Lee, H. (2002). Discrimination of geochemical compositions between the Changjiang and the Huanghe sediments and its application for the identification of sediment source in the Jiangsu coastal plain, China. *Mar. Geol.* 186, 229–241. doi:10.1016/s0025-3227(02)00335-3

Yang, C. (1989). Active, moribund and buried tidal sand ridges in the East China Sea and the southern Yellow Sea. *Mar. Geol.* 88, 97–116. doi:10.1016/0025-3227(89)90007-8

Ye, H., Fang, X., and Wang, W. (1988). *Atlas of natural Resources of Jiangsu coastal zone*. Beijing: Science Press.

Ye, L., Yu, G., Liao, M., and Li, Y. (2016). Dynamic simulations of the late MIS 3 transgressions in the East China Sea and southern Yellow Sea, China. *Acta Oceanol. Sin.* 35, 48–55. doi:10.1007/s13131-016-0919-5

Yin, Y., and Zhang, N. (2010). Sedimentary environments of Xiyang tidal channel of radial tidal sand ridge system since the late period of Late Pleistocene in South Yellow Sea. *J. Palaeogeogr.* 12, 618–628. in Chinese with English abstract.

Yin, Y., Zou, X., Zhu, D., and Huang, J. (2008). Sedimentary facies of the central part of radial tidal sand ridge system of the eastern China coast. *Front. Earth Sci. China* 2, 408–417. doi:10.1007/s11707-008-0053-6

Yin, Y., Jia, P., and Li, Q. (2016). "Sedimentary facies and Late Pleistocene-Holocene evolution of the northern Jiangsu coast and radial tidal ridge field, South Yellow Sea, China," in *Contributions to modern and ancient tidal sedimentology: Proceedings of the tidalites 2012 conference* (John Wiley & Sons), 293–312.

Yoshikawa, S., and Nemoto, K. (2014). The role of summer monsoon-typhoons in the formation of nearshore coarse-grained ripples, depression, and sand-ridge systems along the Shimizu coast, Suruga Bay facing the Pacific Ocean, Japan. *Jpn. Mar. Geol.* 353, 84–98. doi:10.1016/j.margeo.2014.03.018

Yu, Ge, Liangtao, Ye, and Liao, Mengna (2016). Simulations of coastal sediment patterns during the late Pleistocene in Jiangsu coasts(in Chinese with English abstract). *Acta Sedimentol. Sin.* 34, 670–678.

Zhang, C., Zhang, D., Zhang, J., and Wang, Z. (1999). Tidal current-induced formation-storm-induced change-tidal current-induced recovery-Interpretation of depositional dynamics of formation and evolution of radial sand ridges on the Yellow Sea seafloor. *Sci. China Ser. D.* 1, 3–14. doi:10.1007/bf02878492

Zhang, Z., Xie, L., Zhang, Y., Xu, J., Li, S., and Wang, Y. (2010). Sedimentary records of the MIS 3 transgression event in the North Jiangsu Plain, China. *Quat. Sci.* 30 (5), 883–891. in Chinese with English abstract. doi:10.3969/j.issn.1001-7410.2010.05.05

Zhang, C., Yang, Y., Tao, J., Chen, Y., Yao, P., and Su, M. (2013). Suspended sediment fluxes in the radial sand ridge field of South Yellow Sea. *J. Coast. Res.* 65, 624–629. doi:10.2112/si65-106.1

Zhang, X., Zhang, Z., Lan, X., and Li, R. (2013). *Regional geology of south Yellow sea*. Beijing: China Ocean Press. in Chinese.

Zhang, X., Ge, C. D., Yin, Y., Lu, Y. M., and Li, H. Q. (2014). The geochemical characteristic and sedimentary environment evolution of the Dabeicao channel and Dongsha shoal area among the radial tidal sand ridge system, southern Yellow Sea. *J. Nanjing Univ. (Nat. Sci.)* 50, 538–552. in Chinese with English abstract.

Zhang, L., Qin, X., Liu, J., Sun, C., Mu, Y., Gao, J., et al. (2016). Geochemistry of sediments from the huaibei plain (east China): Implications for provenance, weathering, and invasion of the Yellow River into the Huaihe River. *J. Asian Earth Sci.* 121, 72–83. doi:10.1016/j.jseaes.2016.02.008

Zhang, R. (1984). Land-forming history of the Huanghe River delta and coastal plain of north Jiangsu (in Chinese with English abstract). *Acta Geogr. Sin.* 39, 173–184.

Zhang, R. (1988). Evolution of coastal zone in jiangsu province after the Huanghe river changed its lower course. *J. Nanjing Univ. (Geogr.)* 9, 22–31. in Chinese with English abstract.

Zhao, S. (1991). Melt origin of fault-generated pseudotachylytes demonstrated by textures. *Mar. Geol. Quat. Geol.* 11, 105–112. doi:10.1130/0091-7613(1983)11<105:moofpd>2.0.co;2

Zhou, L., Liu, J., Saito, Y., Zhang, Z., Chu, H., and Hu, G. (2014). Coastal erosion as a major sediment supplier to continental shelves: example from the abandoned old huanghe (Yellow River) delta. *Cont. Shelf Res.* 82, 43–59. doi:10.1016/j.csr.2014.03.015

Zhu, Y., and Chang, R. (2001). Sediment dynamics study on the origin of the radial sand ridges in the southern Yellow Sea. *Stud. Mar. Sin.* 43, 38–50. in Chinese with English abstract.

Zhu, Y. (1998). New development of studies on origin of radiating sand ridges in the south Yellow Sea. *Mar. Geol. Quat. Geol.* 18, 113–118. in Chinese with English abstract.